Copy No. ____

TRANSFORMATION TOUGHENING OF CERAMICS

ANNUAL REPORT NO. 2 FOR THE PERIOD
January 15, 1990 through January 11, 1991

CONTRACT NO. F49620-89-C-0031

Prepared for:

Air Force Office of Scientific Research
Directorate of Electronic and Material Sciences
Building 410
Bolling, AFB, DC 20332-6448

D.B. Marshall
Principal Investigator

FEBRUARY 1991

Rockwell International

REPORT DOCUMENT PAGE

Form Approved
OMB No. 0704-0188

1. AGENCY USE ONLY *(Leave blank)*	2. REPORT DATE	3. REPORT TYPE AND DATES COVERED
	FEBRUARY 1991	ANNUAL REPORT - 1/15/90 - 1/14/1991

4. TITLE AND SUBTITLE

TRANSFORMATION TOUGHENING OF CERAMICS

5. FUNDING NUMBERS

F49620-89-C-0031

6. AUTHOR(S)

D.B. MARSHALL

7. PERFORMING ORGANIZATION NAME(S) AND ADDRESS(ES)

ROCKWELL INTERNATIONAL
Science Center
1049 Camino Dos Rios
Thousand Oaks, CA 91360

8. PERFORMING ORGANIZATION REPORT NUMBERS

SC71002.AR

9. SPONSORING/MONITORING AGENCY NAME(S) AND ADDRESS(ES)

Air Force Office of Scientific Research
Bolling Air Force Base
Washington, D.C. 20332
Attn: Dr. Liselotte J. Schioler

NE

10. SPONSORING/MONITORING AGENCY REPORT NUMBER

3306/A3

11. SUPPLEMENTARY NOTES

12a. DISTRIBUTION AVAILABILITY STATEMENT

UNLIMITED

12b. DISTRIBUTION CODE

13. ABSTRACT *(Maximum 200 words)*

14. SUBJECT TERMS

Ceramics, Zirconia, Toughening, Mechanical Properties, R-Curve Behavior, Fracture Mechanics, Transformation, Fatigue

15. NUMBER OF PAGES

16. PRICE CODE

17. SECURITY CLASSIFICATION OF REPORT	18. SECURITY CLASSIFICATION OF THIS PAGE	19. SECURITY CLASSIFICATION OF ABSTRACT	20. LIMITATION OF ABSTRACT
UNCLASSIFIED	UNCLASSIFIED	UNCLASSIFIED	UNLIMITED

TABLE OF CONTENTS

A-1

ABSTRACT

The transformation strains responsible for toughening of ZrO_2 materials have been measured directly using Moiré interferometry and a high resolution strain mapping technique based on digital image correlation. Results were correlated with Raman spectroscopy and finite element calculations. Calculations of the crack tip shielding in Ce-ZrO_2 indicated that the fracture toughness could be increased by a factor of 2 by modifying the microstructure to change the shape of the transformation zone ahead of the crack tip. Layered composites of Ce-ZrO_2 and Al_2O_3/Ce-ZrO_2 have been explored as a means of achieving such zone modifications. Using a colloidal technique, multi-layered composites with layer thickness as small as 10 μm have been fabricated. These layered structures have been observed to interact much more strongly than expected with the transformation zones, causing widening of the zone to the side of the crack as well as modification of the frontal region. The potential exists for extremely high fracture toughness in such systems.

1.0 INTRODUCTION

The goal of this research is to develop a basic scientific understanding of factors that dictate the mechanical properties of transformation toughened ceramics and to use that understanding to design and fabricate microstructures with improved properties. Our approach is to develop and use new methods, such as Raman spectroscopy and high resolution strain measurement techniques, to measure transformation characteristics directly within zones surrounding crack tips, and hence, in combination with mechanics modeling to deduce the toughening mechanisms and relationships between microstructural characteristics and macroscopic properties. With the guidance and insight gained from such experiments, new microstructures are being designed to optimize the desirable properties. Detailed results of the research done during the past year are contained in papers that are included as Sects. 3 to 6 of this report, and which have been published in or submitted to the journals noted on the cover pages. The results of these as well as some other ongoing work are briefly summarized below.

Direct measurements of the residual strains that are responsible for crack tip shielding have been obtained within the transformation zones surrounding cracks in Mg-PSZ using two techniques (Sect. 3): Moiré interferometry and high resolution strain mapping by digital image correlation. Both methods provide maps of differential in-plane displacements within the specimen surface that is intersected by the crack, the latter method with the higher resolution (by about an order of magnitude). The results were compared with finite element analysis to assess surface relaxation effects, and the measured strains were used to evaluate the crack tip stress intensity factor. The calculated shielding, assuming that the net transformation strain was only the hydrostatic component, was consistent with the equivalent calculation using Raman measurements. However, both were smaller than the observed toughening. An approach for determining the shielding contribution due to nonhydrostatic strain components, using in-plane and out-of-plane residual strain measurements with finite element modeling, was outlined. Most of the strain measurements were done during the previous year of this contract, with the detailed FEM analysis, additional Raman spectroscopy and correlation with measurements being completed during the past year.

Several other studies directed towards understanding the nature of the phase transformation responsible for toughening are in progress. A shape-memory effect has been observed by heat treating Mg-PSZ compact tension specimens containing cracks to remove the transformation zone (i.e., transform monoclinic particles within the transformation zone to the tetragonal phase). The subsequent retransformation during ambient temperature aging (over periods of several months) has been monitored by measuring changes in crack opening displacements and correlating them with direct measurements of transformation by Raman spectroscopy and out-of-plane displacement measurements (Sect. 4). Further detailed measurements are being made of in-plane and out-of-plane transformation strains in Mg-PSZ to allow direct distinction between hydrostatic and nonhydrostatic strains. Collaboration is continuing with Professors R. McMeeking and A.G. Evans of University of California at Santa Barbara to simulate resistance curves for subcritical transformation by finite element analysis, using as input some of the Raman measurements of steady state zone characteristics. Such simulation will provide valuable insight into the initiation condition for transformation.

Calculations of the crack tip shielding due to transformation zones with the unusual elongated shapes observed in Ce-TZP ceramics are presented in Sect. 5. Raman studies of the transformation zone characteristics were also done in collaboration with Professor D. Shetty. High fracture toughnesses (in the range 12-20 $MPa \cdot m^{1/2}$) have been observed in these materials, in which the transformation zone extends ahead of the crack a distance ~ 10 to 20 times the zone width (this shape contrasts with that of other ZrO_2 ceramics where the zone extends approximately equal distances ahead and to the side of the crack). Two important conclusions were drawn from the results: (1) the calculated stress intensity factors confirmed that the measured fracture toughness in Ce-TZP is consistent with the toughening being due to crack shielding from the observed transformation zones - this contrasts with speculation in the literature that crack tip shielding is not responsible for the toughening, but instead, a Dugdale zone mechanism operates; (2) given that transformation shielding is responsible for the observed toughening, the calculations show that if the microstructure could be modified to eliminate the elongation of the zone ahead of the crack, the toughness could be increased by a factor of approximately 2, making these the highest toughness ceramics known.

Based on these calculations and our understanding of the formation and arrest of autocatalytic transformation bands in Mg-ZrO_2 ceramics, several types of dual scale microstructures in Ce-ZrO_2 have been fabricated and tested with some remarkable results (Sect. 5). These dual scale microstructures contained barriers to transformation with a spatial scale ~ 100 times the grain diameter, in the form of either A_2O_3 platelets or Al_2O_3 layers (or Al_2O_3/ZrO_2 mixture). The layered composites exhibited toughening effects much larger than we expected (Sect. 5); as well as preventing the detrimental autocatalytic transformation directly ahead of the normally incident crack, the layers caused extensive widening of the transformation zone normal to the crack (which is beneficial to toughening). The enhanced widening effect is not yet fully understood, but is most likely due to both the nontransformability and the higher elastic modulus of the Al_2O_3 layers. The layered composites were fabricated using a colloidal method developed in collaboration with Professor F.F. Lange (U.C. Santa Barbara). The technique has been used to produce layers with thickness as small as 10 μm, an order of magnitude smaller than that of conventional tape casting methods used to fabricate multilayered structures.

Further development of this and related systems will continue in 1991. Our initial observations and development of the fabrication technique for layered composites were done with a commercial Ce-ZrO_2 material that has relatively small transformation zones in the absence of our layered structured. Composites are being fabricated with Ce-ZrO_2 supplied by Dr. R. Cutler of Ceramatec, which exhibit the very large zones and higher toughness. The transformation zone enhancement observed in layered composites is also expected in composites containing continuous Al_2O_3 fibers in Ce-ZrO_2 matrix. Such composites are being fabricated using sapphire fibers.

2.0 PUBLICATIONS, PERSONNEL AND TECHNICAL PRESENTATIONS

2.1 Publications

(a) Publications in press or in preparation from work done in 1990:

1. "Direct Measurement of Transformation Zone Strains in Toughened Zirconia," by M.S. Dadkhah, D.B. Marshall, W.L. Morris and B. Cox, J. Am. Ceram. Soc., in press.

2. "Enhanced Toughening in Layered ZrO_2 Microstructures," by D.B. Marshall, F.F. Lange and J.R. Ratto, in preparation for J. Am. Ceram. Soc.

3. "Transformation Recovery in Mg-RSZ after High Temperature Annealing," by M.C. Shaw, D.B. Marshall and A.H. Heuer, in preparation for J. Am. Ceram. Soc.

4. "Resistance Curve Simulations in Transformation Toughened Materials," by C.L. Hom, R.M. McMeeking, A.G. Evans and D.B. Marshall, in preparation for J. Am. Ceram. Soc.

(b) Publications in print 1989 and 1990:

1. "Crack Shielding in Ceria-Partially Stabilized Zirconia," by D.B. Marshall, J. Am. Ceram. Soc. 73(10), 3119-21 (1990).

2. "Crack Tip Transformation Zones in Toughened Zirconia," by D.B. Marshall, M.C. Shaw, R.H. Dauskardt, R.O. Ritchie, M. Readey and A.H. Heuer, J. Am. Ceram. Soc. 73(9), 2659-66 (1990).

3. "Cyclic Fatigue Crack Propagation in Mg-PSZ Ceramics," by R.H. Dauskardt, D.B. Marshall and R.O. Ritchie, J. Am. Ceram. Soc. 73(4), 893-903 (1990).

4. "On the Thermoelastic Martensitic Transformation in Tetragonal ZrO_2 by A.H. Heuer, M. Ruhle and D.B. Marshall, J. Am. Ceram. Soc. 73[4] 1084-93 (1990).

5. "Reversible Transformation and Elastic Anisotropy in Mg-PSZ," by D.B. Marshall and M.V. Swain, J. Am. Ceram. Soc. 72[8], 1530-32 (1989).

6. "Cyclic Fatigue-Crack Propagation in Ceramics: Behaviour in Overaged and Partially Stabilized MgO-ZrO_2," by R.H. Dauskardt, D.B. Marshall and R.O. Ritchie, Mat. Res. Soc. Proc. on Fracture Mechanics of Structural Ceramics, 1989.

7. "Structural and Mechanical Property Changes in Toughened Mg-PSZ at Low Temperatures," by D.B. Marshall, M.R. James and J.R. Porter, J. Am. Ceram. Soc. 72[2], 218-27 (1989).

2.2 Personnel

The principal investigator is Dr. D.B. Marshall. Other contributors from the Rockwell Science Center were Dr. M. Dadkhah, Dr. W.L. Morris, Dr. B.N. Cox, Mr. M. Shaw (also a part time graduate student at U.C. Santa Barbara), Mr. E. Wright and Mr. J. Ratto. The program has also benefitted from several informal collaborations with universities: Professors F.F. Lange, R. McMeeking and A.G. Evans and graduate student C.L. Hom, from U.C. Santa Barbara; Dr. R.H. Dauskardt and Prof. R.O. Ritchie from U.C. Berkeley; and Prof. A.H. Heuer and Dr. M. Readey from Case Western Reserve University.

2.3 Technical Presentations

1990

1. Albrecht-Rabenau Symposium on Ceramic Science, Max-Plank-Institute (Tegernsee), June 1990 invited lecture, "Modeling of Mechanical Properties."

2. American Ceramic Society Annual Meeting, Dallas, April 1990, invited lecture, "Transformation Zones in ZrO_2."

1989

1. 4th International Conference on Science and Technology of Zirconia, Anaheim, Nov. 1989, Invited keynote speaker: "Crack Tip Zones in Transformation Toughened Ceramics."

2. 3rd Int. Conf. on Fundamentals of Fracture, Irsee, Germany, June 1989, Invited speaker: "Crack Tip Zones in Transformation Toughened Ceramics."

3. American Ceramic Society Annual Meeting, Indianapolis, April 1989, "Characterization of Transformation Zones in Toughened Zirconia."

4. 13th Annual Conf. on Composites and Advanced Ceramics, Cocoa Beach, Jan. 1989, "Cyclic Fatigue Crack Propagation in Advanced Ceramics."

3.0 DIRECT MEASUREMENT OF TRANSFORMATION ZONE STRAINS IN TOUGHENED ZIRCONIA

J. Am. Ceram Soc., in press.

DIRECT MEASUREMENT OF TRANSFORMATION ZONE STRAINS IN TOUGHENED ZIRCONIA

M.S. Dadkhah, D.B. Marshall, W.L. Morris and B.N. Cox

Rockwell Science Center
1049 Camino Dos Rios
Thousand Oaks, CA 91360

ABSTRACT

Residual strains responsible for crack tip shielding have been measured within transformation zones surrounding cracks in Mg-PSZ. Two techniques were used for strain measurement: moiré interferometry and high resolution image matching. Both methods provide maps of differential in-plane displacements within the specimen surface intersected by the crack, the latter method with the higher resolution. The results are compared with finite element analysis to assess surface relaxation effects, and the measured strains are used to evaluate the crack tip shielding stress intensity factor. Calculations based on the assumption that the unconstrained transformation strain is hydrostatic dilatation yielded results that were significantly smaller than the measured toughness increases.

J10585HD/bjc

1.0 INTRODUCTION

The high fracture toughness of certain zirconia containing ceramics has been attributed to shielding of crack tips by transformation strains.[1-10] The strains result from shape changes associated with the martensitic tetragonal-to-monoclinic transformation within limited zones surrounding the cracks. The existence of such zones has been detected by several techniques: x-ray diffraction,[6,11-14] transmission electron microscopy,[6,15,16] and Raman spectroscopy,[17-21] all of which detect the presence of the monoclinic transformation product.

If the net transformation strain was known unambiguously, these zone measurements would allow calculation of the degree of crack tip shielding, and hence, a direct comparison of transformation toughening theory and experimental toughness measurements.[10,22-27] The transformation strain is composed of both shear (16%) and dilatational (4%) components.[2,8,10] However, the long-range shear component can be partly, or completely, relieved by twinning in the monoclinic product, thus introducing an uncertainty of approximately a factor of two in calculating the toughening.[10] Elimination of this uncertainty requires techniques that provide direct measurement of transformation strains within the crack zone. Indirect measurements of the strains have been obtained from optical interference measurements of out-of-plane surface distortions due to the transformation strains.[21,28-31] In this paper, we present measurements by high resolution displacement mapping and moiré interferometry of transformation strains normal to the crack plane within the wake of the crack. This technique could potentially be used, in conjunction with out-of-plane displacement measurements and finite element modeling, to deduce the net transformation strain directly. In the present work, preliminary measurements and finite element analysis are used to evaluate the crack tip shielding, assuming purely dilatational strain.

2.0 EXPERIMENTAL

2.1 Materials and Crack Growth Experiments

The test material was a partially stabilized zirconia containing 9% MgO (MgPSZ), as used in previous studies.[20,21] Fabrication, heat-treatment and microstructure are described by Hannink,[32] and Hannink and Swain.[7] Two final heat treatments, which involved subeutectoid annealing at 1100°C, were used to make materials with steady-state fracture toughnesses of 12 and 16 MPa•m$^{1/2}$. The microstructures were composed of cubic ZrO_2 grains of ~ 50 μm diameter, containing lens-shaped tetragonal and monoclinic precipitates (~ 40% by volume) with largest dimension ~ 300 nm. Recent study has shown that the subeutectoid heat treatment used to manipulate the stability of the tetragonal precipitates (and hence the toughness) also causes formation of a large amount of the δ-phase, $Mg_2Zr_5O_{12}$, both at the precipitate boundaries and throughout the matrix.[33]

Cracks were grown stably under measured loading conditions in compact tension fracture mechanics specimens of dimension 25 × 30 × 2 mm. A loading fixture that could attach to the stage of an optical microscope was used, to allow in situ observation of the crack tip and wake zones by several techniques.

2.2 Out-of-Plane Displacement Measurements

Out-of plane displacements of the specimen surface adjacent to the crack (u_2 in Fig. 1) were measured by optical interference microscopy. The interference measurements were obtained from the surface of the compact tension specimen which had been polished flat prior to introduction of the crack.

2.3 In-Plane Strain Measurements

Transformation strains, e_1^S, , normal to the crack plane (Fig. 1) were measured by two techniques (the superscript S denoting strains measured at the specimen surface). One technique was moiré interferometry,[34] which involved gluing a diffraction grid to the surface of the compact tension specimen before growing the crack, and then, during loading to extend the crack, illuminating the surface with a He-Ne laser (wavelength 632 nm) in the configuration of Fig. 2. In this set up, half of the incident beam impinged directly onto the specimen surface, while the other half, after reflection from a plane mirror, was incident in a symmetrical direction to produce a virtual reference grating. The combination of this reference grating and the diffraction grating bonded to the specimen produced the moiré pattern, which was recorded photographically. The moiré pattern consists of a set of fringes, which represent contours of constant displacement in the x_1 direction, the increment between adjacent fringes being equal to the period of the reference grating (0.417 μm). In the present experiments, this technique allowed strain resolution of 10^{-3} over gauge lengths as small as 40 μm.

The second technique of in-plane strain measurement entailed digital image matching of high magnification optical micrographs, taken from the surface of the compact tension specimen before and after passage of the crack. The image matching provides maps of relative displacements of corresponding features within the "before" and "after" images. This technique (referred to as HASMAP) has been described more fully in reference 35. In the present experiments, the specimen surface, which had been highly polished after heat treatment, was coated with a thin (~ 100Å) layer of gold then decorated with submicron MgO crystallites (from smoke of burning Mg) which provided the reference features for image matching. Then a set of optical micrographs were obtained from the regions ahead of the notch while the specimen was in the loading

fixture, before the load was applied. After applying the load and growing a crack of sufficient length to reach steady state (in toughness and transformation zone size), another set of micrographs, which exactly matched the first set in position and imaging conditions, was obtained. Analysis of these micrographs provided x_1-x_3 displacement maps with relative displacement resolution of ~ 100Å (substantially smaller than the point-to-point image resolution). The usable gauge length for strain measurement was as small as 10 μm, substantially smaller than that achievable by moiré interferometry.

3.0 EXPERIMENTAL RESULTS

3.1 Moiré Interferometry

Moiré interference micrographs from a compact tension specimen containing a steady-state crack are shown in Figs. 3(a) and 3(b). The crack was grown stably from the notch a distance of 5 mm, unloaded (Fig. 3(a)), then reloaded and extended a further 1.7 mm (Fig. 3(b)). The steady-state fracture toughness was 16 MPa•$m^{1/2}$. In other specimens that were subjected to the same heat treatment in an earlier study,[21] increasing crack resistance curves for the initial 1-2 mm of crack extension and transformation zones of ~ 1 mm in width (from Raman spectroscopy) were reported.

The fringes in Figs. 3(a) and 3(b) represent contours of constant displacement in the direction x_1 normal to the crack. Therefore, in these micrographs, an area of constant normal strain, e_1^S, in the x_1 direction would give rise to equally spaced horizontal fringes; an area of pure rotation or shear, e_{12}^S, would cause equally spaced vertical fringes; and areas of mixed normal strain e_1^S and either rotation or shear would give inclined fringes. (To distinguish rotation and shear a second moiré image would be needed with the plane of incidence of the laser rotated by 90°). Several zones

surrounding the crack in Fig. 3 can be identified. Behind the crack tip and far from the crack plane (top left and bottom left of the micrographs), nearly pure rotation (or shear strain) is evident, whereas adjacent to the crack plane in the wake region, there is mixed rotation and normal strain, with the normal strain component e_1^S being tensile. Surrounding the tensile region is a zone in which e_1^S is compressive. The compressive strains are caused by Poisson's contraction, associated with out-of-plane displacements of material outside the transformation zone (see Sect. 4).

The out-of-plane displacements were measured from optical interference micrographs (Fig. 4(a)) obtained from the wake region of the crack in Fig. 3. The fringes in Fig. 4(a) represent contours of constant separation of the specimen surface and an inclined reference mirror: equally spaced horizontal fringes represent a flat specimen surface, whereas the fringe deflections towards the bottom of the micrograph indicate surface uplift. The narrow region (~ 20 μm width) immediately adjacent to the crack in Fig. 4(a), where the fringes deflect in the opposite direction, towards the top of the micrograph, is due to deformation of the moiré grid and glue, and corresponds to the region in Figs. 3(a) and 3(b) near the crack where the moiré fringes become indistinct.

The residual in-plane and out-of-plane displacements, u_1 and u_2, obtained from the steady-state wake region of Figs. 3(b) and 4(a), are compared in Fig. 4(b); the distances from the crack plane over which u_1 and u_2 are non-zero are similar. The corresponding variation of the normal strain e_1^S with distance from the crack is shown in Fig. 4(c). Also plotted in Fig. 4(c) is the result of a finite element calculation that takes into account the effects of surface relaxation on the strains e_1^S (see Section 4).

3.2 High Resolution Displacement Field Mapping

The image matching technique was used for generating in-plane displacement maps for the lower toughness material; because of its smaller transformation zone, the higher resolution of this method was needed to obtain information from within the zone. Optical interference micrographs from the steady-state crack used for analysis are shown in Figs. 5(a) and 5(b); these micrographs were obtained with the reference mirror parallel to the undistorted specimen surface, so that the fringes represent contours of constant out-of-plane displacement, at increments of Δu_2 = 270 nm. The degree of uplift in the uniform wake zone (approximately 0.8 μm adjacent to the crack) and the measured steady-state fracture toughness, K_c = 12 MPa•$m^{1/2}$, are the same as in nominally identical materials used in two previous studies,[20,21] and referred to therein as "mid-toughened." Rows of indentations visible in Figs. 5(a) and 5(b) near the crack were introduced using a Vickers indenter at 2N load, to provide references for precise alignment of the micrographs taken before and after crack growth.

Results of the displacement analysis from the region adjacent to the crack in Fig. 5(b) are shown in Fig. 5(c). The strains e_1^S normal to the crack are plotted on the vertical axis, and the x_1-x_3 plane corresponds to the area marked on Fig. 5(b). The actual micrographs used for analysis (not shown) were obtained at magnification of 280 using a X25 objective lens with numerical aperture 0.45. The residual strain e_1^S is tensile within approximately 50 μm of the crack and compressive beyond. The strain distribution is qualitatively similar to the result from moiré interferometry from the higher toughness material, but the zone width is smaller.

The magnitude of the strain adjacent to the crack is quite variable at different locations along the wake. The amplitudes of the variations are about an order of magnitude larger than the sensitivity of the measurements. Moreover, there is a one-to-

one correspondence between the nonuniformity of the strain e_1^S and areas in Fig. 5(b) where the out-of-plane displacements are larger than average (as indicated by the bulges in the interference fringes adjacent to the crack). These variations in out-of-plane displacements along the line of the crack are also evident in Nomarski interference (which highlights changes in angle of the specimen surface) when the direction of apparent illumination is along the crack (Fig. 6). These correlations provide confidence that the nonuniformity of e_1^S in Fig. 5(c) is not an artifact due to an unidentified error in measurement.

The displacements corresponding to Fig. 5(c), measured along a set of 12 equally spaced lines normal to the crack, are shown in Fig. 7(a). The average in-plane displacements from Fig. 7(a) at each distance from the crack are compared with the average out-of-plane displacements from Fig. 5(b) in Fig. 7(b). The results are qualitatively similar to those in Fig. 4(b) for the higher toughness material, but the width of the zone of residual displacements is smaller. The average in-plane strains e_1^S are shown in Fig. 7(c), along with a finite element calculation taking into account free surface relaxation (see Section 4).

4.0 ANALYSIS OF SURFACE DISPLACEMENTS AND STRAINS

The shielding of the crack tip by a transformation zone has been expressed in terms of the unconstrained transformation strains within the zone (see Sect. 5). In the interior of the specimen, where uniaxial strain conditions exist within a steady-state wake zone formed by hydrostatic dilatational transformation, the unconstrained transformation strains are related straightforwardly to the residual strain in the wake.

For transformation with hydrostatic dilatation e^T, the residual strain normal to the crack plane is (Appendix)

$$e_1^I = \left(\frac{1 + \nu}{1 - \nu}\right) \frac{e^T}{3} \quad , \tag{1}$$

where ν is Poisson's ratio and the superscript I denotes a position adjacent to the crack plane in the interior of the specimen. However, experimental strain measurements by techniques reported here are restricted to the specimen surface and are influenced by surface relaxation, as indicated schematically in Fig. 1. At the edge of the crack, uniaxial stress conditions exist and, for the dilatational transformation, the residual strain normal to the crack is (Appendix)

$$\varepsilon_1^S = (1 + \nu)\, e^T/3 \quad . \tag{2}$$

Further from the crack, analytical solutions relating the surface strains to e^T are not available. Therefore, to evaluate the effect of surface relaxation in this region, finite element calculations were done (using the program ABAQUS) for the geometry shown in Fig. 8(a) (inset), which simulates a transformation zone of width w, within which the unconstrained transformation strain $e^T(x_1)$ is a function of distance x_1 from the crack plane, but is uniform in the directions x_2 and x_3 over the wake of the crack. The following boundary conditions were imposed; normal displacements $u_3 = 0$ everywhere, normal displacements u_1 and u_2 zero along the right and bottom edges respectively, and normal stresses zero along the crack and specimen surfaces. Elements within a distance w of the crack plane were given a hydrostatic dilatational transformation strain (some results for nonhydrostatic strain are given in the Appendix) with magnitude unity

adjacent to the crack and decreasing to zero at $x_1/w = 1$, as shown in Fig. 8(c). The function in Fig. 8(c) was obtained by assuming that $e^T(x_1)$ is proportional to the volume fraction of material transformed at x_1, as measured by Raman microprobe spectroscopy on similar materials.[21] Alternatively, we could have taken various trial functions for $e^T(x_1)$ and chosen the function that gave closest agreement between calculated and measured values of $e_1^S(x_1)$, as described in Ref. 31. Then, comparison of the optimum function with the Raman measurements would provide an independent experimental verification of the consistency of the strain and Raman measurements and the assumption that the transformation strain is proportional to the volume fraction of material transformed. With the procedure used here, comparison of the calculated and measured strains $e_1^S(x_1)$ affords a similar verification.

Computed displacements and strains are shown in Figs. 8(a) and 8(b) for $\nu = 0.3$. The in-plane and out-of-plane displacements, u_1^S and u_2^S, are qualitatively similar to the experimental results of Figs. 4(b) and 7(b). The strain e_1 adjacent to the crack plane (i.e., at $x_1 = 0$) is consistent with Eq. (1) at the interior and Eq. (2) at the top corner. The magnitude of the strain e_1^I in the interior decreases with distance from the crack plane, to zero at the edge of the zone. However, the strain e_1^S at the surface decreases to zero, and becomes compressive, within the zone, with the maximum compressive strain occurring close to the edge of the zone ($x/w = 1$). Therefore, the experimentally observed compressive residual strains outside the region of residual tensile strains are accounted for by surface relaxation. It is also noteworthy that the surface relaxations are such that the net displacement of the edge of the crack is negative (i.e., <u>increased</u> separation of the crack surfaces), whereas in the interior of the specimen, the net displacement is of course positive (i.e., closure).

The computed strain distributions $e_1^S(x_1)$ are compared quantitatively with the experimental measurements in Figs. 4(c) and 7(c), with the values of zone width, w, and transformation strain, $e^T(0)$, adjacent to the crack chosen to give the best fit to the data. For the moiré results from the higher toughness material of Fig. 4(c), the parameters were w = 750 μm and $e^T(0) = 0.01$. With the dilatational component of the transformation strain in the individual transforming particles being $e_0^T = 0.04$, this value of $e^T(0)$ corresponds to a volume fraction of transformed phase of $f = e^T(0)/e_0^T = 0.25$. For the strain mapping measurements from the lower toughness material of Fig. 7(c), the fitted parameters were w = 100 μm and $e^T(0) = 0.01$. In both cases, the computed and measured strain distributions show reasonable agreement. Moreover, the fitted parameters are consistent with values obtained from the abovementioned Raman measurements from similar materials in Ref. 21: w = 900 μm, f = 0.22 for the higher toughness material and w = 200 μm, f = 0.19 for the lower toughness material.

5.0 CRACK TIP SHIELDING

The measured residual strains within the transformation zone can be used directly to calculate the reduction of crack tip stresses due to the transformations and hence, the toughness increase. The reduction in stress at the crack tip is expressed in terms of a shielding stress intensity factor, K_s:[22-24]

$$K_{tip} = K_a - K_s \tag{3}$$

where K_{tip} is the local stress intensity factor at the crack tip and K_a is the applied stress intensity factor. The criterion for crack growth under monotonic loading is taken as a critical value of K_{tip} (i.e., $K_{tip} = K_o$, where K_o is the fracture toughness in the absence of transformation shielding). The corresponding value of K_a ($K_a = K_c = K_o + K_s$) is the fracture toughness measured in the presence of shielding, and K_s is the toughness increase.

For a steady-state crack (i.e., crack growth at constant K_a), with a wake zone of constant width, w, containing a uniform volume fraction, f, of transformed particles, the shielding stress intensity factor under plane strain conditions is[22,23,10]

$$K_s = \frac{AE\, e^T \sqrt{w}}{(1-\nu)} \tag{4}$$

where E is the Young's modulus, e^T is the unconstrained transformation strain of the entire zone ($e^T = fe_o^T$ where e_o^T is the unconstrained transformation strain of the individual transforming particles within the zone), and the constant A is dependent upon the shape of the zone ahead of the crack tip, as well as the nature of the transformation strain. If e^T is isotropic dilatational strain and the frontal zone is defined by a contour of hydrostatic tension in the elastic crack-tip field, then A = 0.22. However, if the frontal zone is semicircular, as suggested by several observations in Mg-PSZ (Fig. 5(a) and Ref. 21), then A = 0.25.

Previous studies of Mg-PSZ[20,21] (see Fig. 8(c)) have shown that the fraction of particles transformed within the zone decreases continuously with increasing distance from the crack (corresponding to a subcritical transformation in the notation of

Ref. 24). In this case, the transformation strain e^T is not uniform. However, provided all the contours of constant e^T around the crack tip and wake are geometrically similar, the shielding stress intensity factor can be obtained by integration of Eq. (4):[21,36,37]

$$K_S = \frac{AE}{(1 - \nu)} \int_0^w e^T(x_1)\, d\sqrt{x_1} \tag{5}$$

where x_1 is the distance from the crack plane. With Eq. (1) this result can be expressed alternatively in terms of the residual strain e_1^I, in the steady-state wake of the crack

$$K_S = \frac{3AE}{(1+\nu)} \int_0^w e_1^I(x_1)\, d\sqrt{x_1} \tag{6}$$

With the finite element results of Fig. 8(a) being used to relate the strains $e_1^S(x_1)$ and $e_1^I(x_1)$, the integral in Eq. (6) was evaluated from the experimentally measured surface strains $e_1^S(x_1)$ of Figs. 4(c) and 7(c). These results, along with the parameters $A = 0.25$ for the semicircular zone front, $E = 200$ GPa and $\nu = 0.25$ give $K_S = 9$ MPa•m$^{1/2}$ for the moiré results from the high toughness material and $K_S = 3$ MPa•m$^{1/2}$ for the strain mapping measurements in the lower toughness material. These results are similar to the values 8.8 and 3.9 MPa•m$^{1/2}$ deduced directly from Raman measurements (also with the assumption of hydrostatic dilatational strain) from nominally identical materials in Ref. 21.

6.0 DISCUSSION

The results described in the previous sections provide direct measurements of transformation strains that are a source of toughening in Mg-PSZ. With the assumption that the net unconstrained transformation strain is hydrostatic dilatation (i.e., long range shear strains are relieved by twinning), we have used the measured residual strain components normal to the crack plane in two materials of different toughness to calculate the crack tip shielding stress intensity factors. The results agree closely with values obtained from similar materials using Raman microprobe measurements of the distributions of transformed monoclinic phase within the transformation zones, with the same assumption of a hydrostatic transformation strain.[21] Both of these calculations also implicitly assumed that the distribution of monoclinic phase within the transformation zone was the same in the plane strain crack tip region in the interior of the specimen as in the near-surface crack tip region where plane stress conditions are approached. Some preliminary Raman microprobe measurements have been done to test this approximation.[38] This entailed growing a crack completely through a compact tension specimen, preparing a polished section normal to both the crack plane and the original surface of the specimen, and measuring the volume fraction of monoclinic phase along scan lines normal to the crack at various depths below the original surface. The results of these scans were not significantly different from those on the original surface.

The assumption of hydrostatic dilatational transformation strain in this and other studies is rationalized mainly on the observation by transmission electron microscopy of extensive twinning in the transformed monoclinic particles within transformation zones.[6,15,17] However, possible thin-foil relaxation effects cast some doubt as to whether such observations are representative of the behavior in bulk material. Moreover, the magnitude of K_s obtained with this assumption, here and in

other studies, does not appear to account fully for the observed toughening: with the values of K_s from Sect. 5 (3 and 9 MPa•m$^{1/2}$) and the measured fracture toughnesses (11 and 16 MPa•m$^{1/2}$), Eq. (3) gives K_o = 7 and 8 MPa•m$^{1/2}$. These values of K_o are substantially larger than expected for the fracture toughness of the material without any toughening. One possible source of this discrepancy is the existence of nonhydrostatic and nonuniform strains in the transformation zone,[10,26] although other toughening mechanisms, such as twin boundary movement as the particles move through the crack tip stress field, crack deflection, or microcracking, are also possible. Experimental methods are needed to distinguish these possibilities.

The techniques used here could potentially be used to determine the deviatoric components of transformation strain within the zone. In-plane residual shear strains e_{13} can be obtained directly from the image matching data that was used to generate the results in Figs. 5 and 7, or from moiré images obtained with two-dimensional gratings. Short-range, nonuniformly distributed shear strains e_{13} were observed from the strain mapping data, but their magnitudes were smaller than 6×10^{-4}, an order of magnitude lower than the strains e_1^S adjacent to the crack. With the transformation of two sets of orthogonally oriented precipitates, an elongation due to shear strain components that is equivalent to plastic deformation on two slip systems is possible, without giving a long-range shear strain e_{13}. In this case, the relative magnitudes of the strain components (e_1^I, e_2^I, e_3^I) of the unconstrained transformation could be determined from comparison of the in-plane and out-of-plane displacements u_1 and u_2. This would involve measurement of u_1 and u_2 as in Figs. 4(b) and 7(b), measurement of the distribution, f(x), of transformed material within the zone by Raman microprobe spectroscopy, and superposition of the finite element solutions of Fig. A1 with the relative magnitudes of e_1^I, e_2^I and e_3^I adjusted so as to build up a zone consistent with both the Raman results and the measured values of u_1 and u_2. Such an analysis was not attempted here

because of the variability in the amount of transformation at different positions along the crack wake (Fig. 7(a)). However, materials with more uniform zones may be amenable to analysis.

7.0 CONCLUSIONS

Moiré interferometry and high resolution strain mapping by image correlation have been used to measure directly the residual transformation strains that exist adjacent to cracks, and are responsible for toughening, in two Mg-PSZ materials. The residual strains were consistent with Raman microprobe measurements of the volume fraction of material transformed. Substantial variability in the residual strains along the crack path was detected. The average strains were used to calculate directly the crack tip shielding stress intensity factor, with the assumption that the unconstrained transformation strain is hydrostatic dilatation. The results are consistent with other equivalent calculations based on Raman microprobe measurements of the distribution of transformed monoclinic phase, which also assumed that only the hydrostatic component of the transformation strain contributes. However, the calculated shielding is significantly smaller than the measured toughness increase, suggesting that either nonhydrostatic components of the transformation strain are significant, or other toughening mechanisms operate. An approach was suggested for resolving this issue using the strain measurement methods described herein.

ACKNOWLEDGEMENTS

Funding for this work was supplied by the U.S. Air Force Office of Scientific Research under Contract No. F49620-89-C-0031.

APPENDIX: RESIDUAL TRANSFORMATION STRAINS

Consider a slab of material adjacent to a crack, as in Fig. 8, which undergoes uniform transformation with unconstrained normal strains (e_1^T, e_2^T, e_3^T). At positions near the crack but far from the specimen surface, the following conditions exist:

$$e_2^I = e_3^I = 0, \quad \sigma_1 = 0 \tag{A1}$$

where e^I is measured relative to the untransformed state. Therefore, the elastic strains e_2 and e_3 are equal to $-e_2^T$ and $-e_3^T$, respectively, and Hook's Law results in:

$$Ee_1 = -\nu\sigma_2 - \nu\sigma_3 \tag{A2}$$

$$Ee_2 = \sigma_2 - \nu\sigma_3 \tag{A3}$$

$$Ee_3 = -\nu\sigma_2 + \sigma_3 \tag{A4}$$

Addition of Eqs. (A3) and (A4) and substitution into Eq. (A2) gives

$$e_1 = \left(\frac{\nu}{1-\nu}\right)\left(e_2^T + e_3^T\right) \tag{A5}$$

for the elastic strain. The total strain e_1^I is the sum of this and the transformation strain:

$$e_1^I = e_1^T + \left(\frac{\nu}{1 - \nu}\right)\left(e_2^T + e_3^T\right) \tag{A6}$$

For hydrostatic dilatation of magnitude $e^T = 3e_1^T$, with $e_1^T = e_2^T = e_3^T$, Eq. (A6) becomes

$$e_1^I = \left(\frac{1 + \nu}{1 - \nu}\right)\frac{e^T}{3} \tag{A7}$$

At the edge of the specimen surface and the crack, the following uniaxial stress conditions exist

$$\sigma_1 = \sigma_2 = 0 \ , \quad e_3^S = 0 \tag{A8}$$

In this case, application of Hook's Law gives

$$e_1^S = e_1^T + \nu e_3^T$$

which, for hydrostatic dilatation becomes

$$e_1^S = (1 + \nu)\, e^T/3 \tag{A9}$$

Results of finite element computations of the strain e_1^s at the specimen surface as a function of distance from the crack plane are shown in Fig. A1 for the three stress-free transformation strains (1,0,0), (0,0,1) and (0,1,0). The results for the more general transformation strain (e_1^T, e_2^T, e_3^T) can be obtained by superposition.

REFERENCES

1. R.S. Garvie, R.H.J. Hannink and R.T. Pascoe, "Ceramic Steel?," Nature 258 703-705 (1975).
2. D.L. Porter and A.H. Heuer, "Mechanisms of Toughening Partially Stabilized Zirconia," J. Am. Ceram. Soc. 60[3-4], 183-84 (1977).
3. F.F. Lange, "Transformation Toughening: Part 5. Effect of Temperature and Alloy on Fracture Toughness," J. Mat. Sci. 17, 255-263 (1982).
4. F.F. Lange, "Transformation Toughening: Part 4. Fabrication, Fracture Toughness and Strength of Al_2O_3-ZrO_2 Composites," J. Mat. Sci. 17, 247-54 (1982).
5. N. Claussen and M. Ruhle, "Design of Transformation Toughened Ceramics," pp. 137-63 in Advances in Ceramics, Vol. 3, Ed., A.H. Heuer and L.W. Hobbs, Am. Ceram. Soc. (1981).
6. M.V. Swain, R.H.J. Hannink and R.C. Garvie, pp. 339-54 in Fracture Mechanics of Ceramics, Vol. 6, edited by R.C. Bradt, A.G. Evans, D.P.H. Hasselman and F.F. Lange, Plenum, NY (1983).
7. R.H.J. Hannink and M.V. Swain, "Magnesia-Partially Stabilized Zirconia: The Influence of Heat Treatment on Thermomechanical Properties," J. Aust. Ceram. Soc. 18[2], 53-62 (1982).
8. A.H. Heuer, "Transformation Toughening in ZrO_2-Containing Ceramics," J. Am. Ceram. Soc. 70[10], 689-698 (1987).
9. A.H. Heuer, M.J. Readey and R. Steinbrech, "Resistance Curve Behavior of Supertough MgO-partially-stabilized ZrO_2 Mat. Sci. Eng. A105/106, 83-89 (1988).
10. A.G. Evans and R.M. Cannon, "Toughening of Brittle Solids by Martensitic Transformations," Acta. Metall. 34[5] 761-800 (1986).

11. K.D. Keefer and T.A. Michalske, "Determination of Phase Transformation Depth Profiles with Synchrotron Radiation," J. Am. Ceram. Soc. 70[4], 227-31 (1987).

12. R.C. Garvie, R.H.T. Hannink and M.V. Swain, "X-Ray Analysis of the Transformed Zone in Partially Stabilized Zirconia (PSZ)," J. Mat. Sci. Lett. 1, 437-40 (1982).

13. T. Kosmac, R. Wagner, and N. Claussen, "X-ray Determination of Transformation Depths in Ceramics Containing Tetragonal ZrO_2," J. Am. Ceram. Soc. 64[4], C72-73 (1981).

14. Y. Mori, Y. Kitano, and A. Ishitani, "X-ray Determination of Transformation Zone Size in Toughened Zirconia Ceramics," J. Am. Ceram. Soc. 71[7], C322-24 (1988).

15. L.H. Schoenlein and A.H. Heuer in Fracture Mechanics of Ceramics, Ed., R.C. Bradt, A.G. Evans, D.P.H. Hasselman and F.F. Lange, Vol. 6, pp. 309-26, Plenum (1983).

16. L.H. Schoenlein, A.H. Heuer and M. Rühle in Advances in Ceramics, Vol. 11, p. 275 (1984).

17. D.R. Clarke and F. Adar, "Measurement of the Crystallographically Transformed Zone Produced by Fracture in Ceramics Containing Tetragonal Zirconia," J. Am. Ceram. Soc. 65[6], 284-88 (1982).

18. R.H. Dauskardt, D.K. Veirs and R.O. Ritchie, "Spatially Resolved Raman Spectroscopy of Transformed Zones in MgO-partially-stabilized Zirconia," J. Am. Ceram. Soc. 72[7], 1124-30 (1989).

19. G. Katagiri, H. Ishida, A. Ishitani, and T. Masaki, "Direct Determination of Transformation Zone Size in Y_2O_3 Containing Tetragonal ZrO_2 Polycrystals by Raman Microprobe"; in Advances in Ceramics, Vol. 24, Science and Technology of Zirconia III. Edited by S. Somiya and N. Yamamoto, Am. Ceram. Soc., Westerville, OH (1988).

20. R.H. Dauskardt, D.B. Marshall and R.O. Ritchie, "Cyclic Fatigue Crack Propagation in Mg-PSZ Ceramics," J. Am. Ceram. Soc., in press.

21. D.B. Marshall, M.C. Shaw, R.H. Dauskardt, R.O. Ritchie, M. Readey and A.H. Heuer, "Crack Tip Transformation Zones in Toughened Zirconia," J. Am. Ceram. Soc, in press.

22. R.M. McMeeking and A.G. Evans, "Mechanics of Transformation Toughening in Brittle Materials," J. Am. Ceram. Soc. 65[5], 242-46 (1982).

23. D.B. Marshall, M. Drory and A.G. Evans, "Transformation Toughening in Ceramics," In Fracture Mechanics of Ceramics, Vol. 6, pp. 289-307, Ed., R.C. Bradt, A.G. Evans, D.P.H. Hasselman and F. Flange, Plenum (1983).

24. B. Budiansky, J.W. Hutchinson and J.C. Lambropoulos, "Continuum Theory of Dilatant Transformation Toughening in Ceramics," Int. J. Solids and Structures 19, 337 (1983).

25. D.M. Stump and B. Budiansky, "Crack Growth Resistance in Transformation Toughened Ceramics," Int. J. Solids Structures 25[6], 635-646 (1989).

26. J.C. Lambropoulos, "Shear, Shape and Orientation Effects in Transformation Toughening." Int. J. Solids Structures 22, 1083-1106 (1986).

27. L.R.F. Rose, "A Kinematical Model for Stress-Induced Transformation Toughening in Brittle Materials," J. Am. Ceram. Soc. 34, 208-11 (1986).

28. M.V. Swain and R.H.J. Hannink, "R-Curve Behavior in Zirconia Ceramics," in Science and Technology of Zirconia II, Advances in Ceramics, Vol. 12, eds., N. Claussen, M. Rühle and A.H. Heuer, Am. Ceram. Soc., Columbus (1984), pp. 225-239.

29. D.B. Marshall, "Strength Characteristics of Transformation-Toughened Zirconia," J. Am. Ceram. Soc. 69[3], 173-180 (1986).

30. D.B. Marshall and M.V. Swain, "Crack Resistance Curves in Magnesia-Partially-Stabilized Zirconia," J. Am. Ceram. Soc. 71[6], 399-407 (1988).

31. B.N. Cox, D.B. Marshall, D. Kouris, and T. Mura, "Surface Displacement Analysis of the Transformed Zone in Magnesia Partially Stabilized Zirconia," J. Eng. Mat. Tech. 110[2], 105-109 (1988).

32. R.H.J. Hannink, "Microstructural Development of Subeutectoid-Aged ZrO_2 Alloys," J. Mater. Sci. 18[2], 457-70 (1983).

33. R.H.J. Hannink: δ Phase During Subeutectoid Annealing.

34. D. Post, "Moiré Interferometry," Chapt. 7, Handbook on Experimental mechanics, Ed., A.S. Kobayashi, Prentice-Hall Englewood Cliffs, NJ (1987).

35. M.R. James, W.L. Morris and B.N. Cox, "A High Accuracy Automated Strain Field Mapper," Exptl. Mechanics, in press.

36. A.G. Evans, D.B. Marshall and N.H. Burlingame, "Transformation Toughening in Ceramics," in Advances in Ceramics, Vol. 3, pp. 202-216, Eds., A.H. Heuer and L.W. Hobbs, The American Ceramic Society, Columbus (1981).

37. C-H Hsueh and P.F. Becker, "Some Considerations of Nonideal Transformation-Zone Profile," J. Am. Ceram. Soc. 71[6], 494-97 (1988).

38. D.B. Marshall and M.C. Shaw, in preparation.

FIGURE CAPTIONS

Fig. 1 Schematic of crack surrounded by dilatational transformation zone.

Fig. 2 Set up for moiré interferometry.

Fig. 3 Moiré interference micrographs from high toughness Mg-PSZ compact tension specimen: (a) crack grown 5 mm from notch then applied load removed, and (b) crack extended further 1.7 mm and applied load held constant while micrograph recorded.

Fig. 4 (a) Two-beam optical interference micrograph (wavelength 540 nm) of surface in Fig. 3 after crack was grown entirely through specimen. Reference mirror tilted so that downward deflection of fringes results from surface uplift. (b) In-plane and out-of-plane displacements from Figs. 3(b) and 4(a). (c) Normal strains e_1^S from data of (b) and finite element results from Fig. 8(a) (see Section 4).

Fig. 5 (a) Optical interference micrograph of mid-toughness Mg-PSZ compact tension specimen containing a crack grown stably under monotonically increasing displacement. Reference mirror parallel to specimen surface so that fringes represent contours of out-of-plane displacement (uplift) (b) Higher magnification from (a) showing area analyzed by HASMAP (using other, higher magnification optical micrographs). (c) Residual strains normal to the crack plane within the area outlined in 5(b).

Fig. 6 Nomarski interference micrographs from the area of Fig. 5(b) at two different specimen orientations.

Fig. 7 (a) Residual displacements from Fig. 5(c), measured along a set of 11 equally spaced lines normal to the crack. (b) Average surface displacements adjacent to the crack in Fig. 5(b): out-of-plane displacements, u_2, from interference micrographs, in-plane displacements from the data used for Figs. 5(c) and 7(a). (c) Average in-plane strains e_1^S from data in Fig. 5(c). Shaded band represents range within which 90% of data fall. Finite element results from Fig. 8(a) (see Section 4).

Fig. 8 Finite element calculations of (a) residual strains normal to crack at the specimen surface (e_1^S) and in the interior of the specimen (e_1^I), (b) Residual in-plane and out-of-plane displacements at the specimen surface. (c) Variation of transformation strain with distance from crack (from Raman microprobe measurements of Ref. 21).

Fig. A1. Finite element calculations of residual strains at the specimen surface resulting from uniaxial unconstrained transformation strains in the three directions x_1, x_2, x_3.

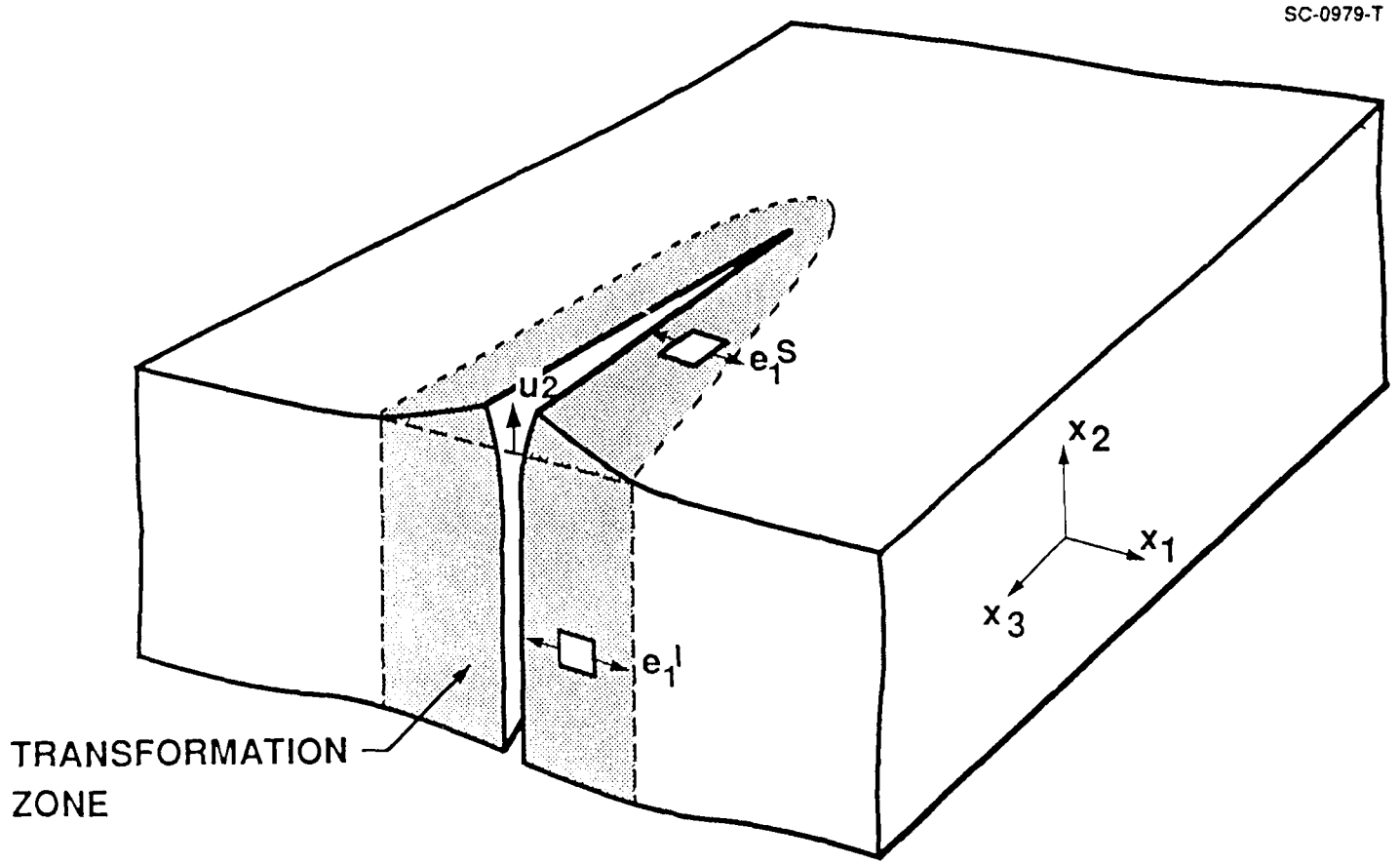
SC-0979-T
u_2
e_1^S
e_1^I
x_2
x_1
x_3
TRANSFORMATION ZONE

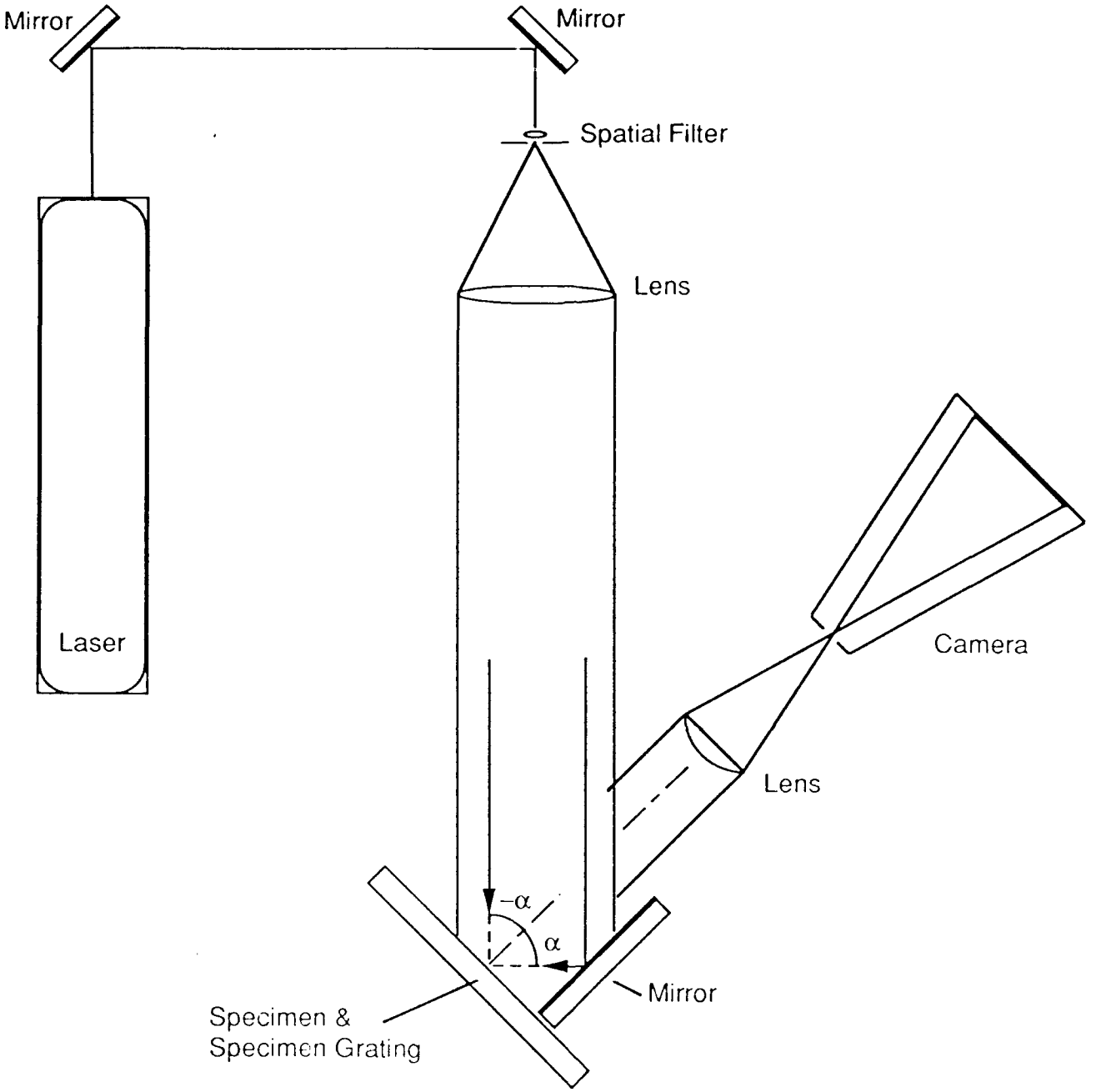
Mirror
Mirror
Spatial Filter
Lens
Laser
Camera
Lens
−α
α
Mirror
Specimen &
Specimen Grating

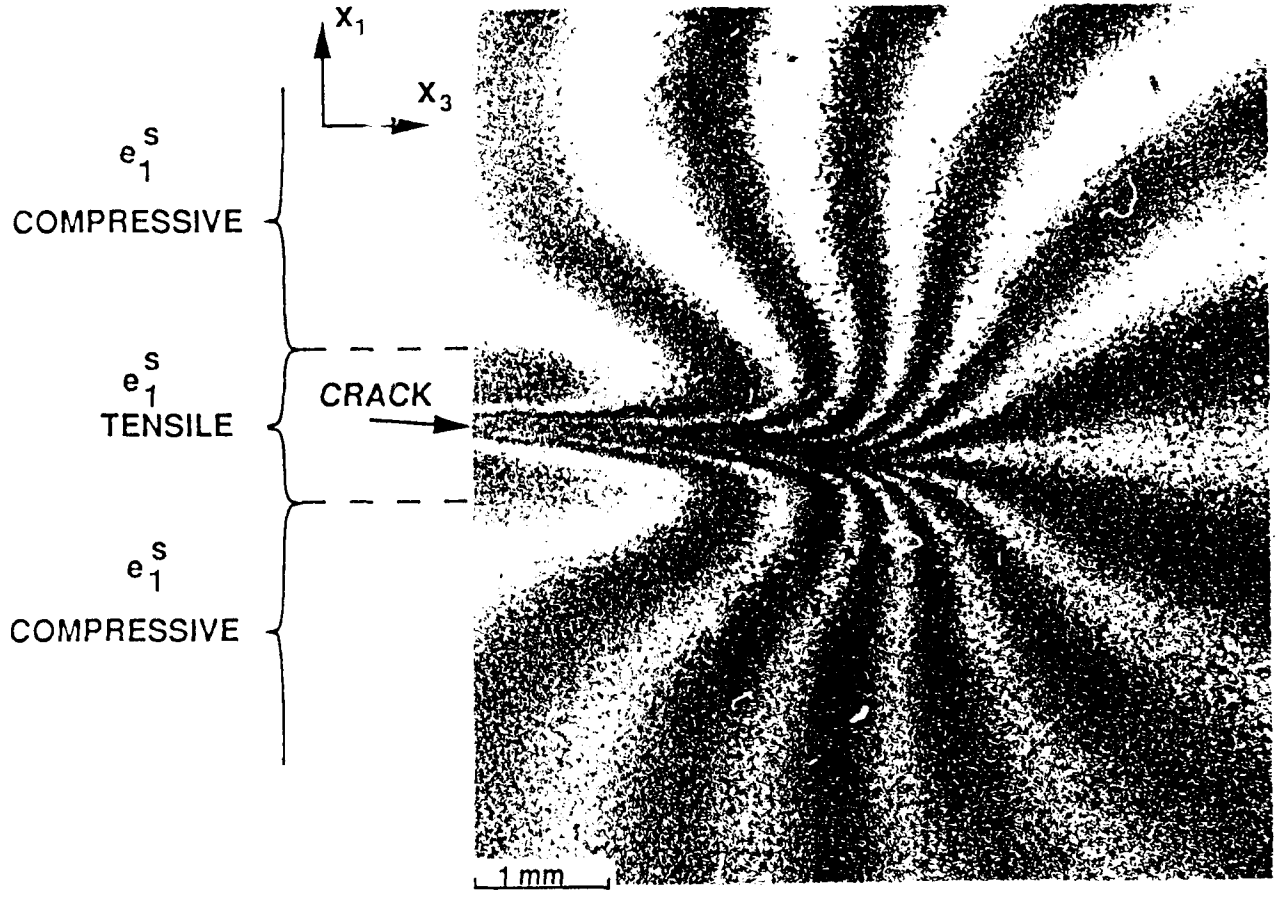
x_1
x_3
e_1^s
COMPRESSIVE
e_1^s
TENSILE
CRACK
e_1^s
COMPRESSIVE
1 mm

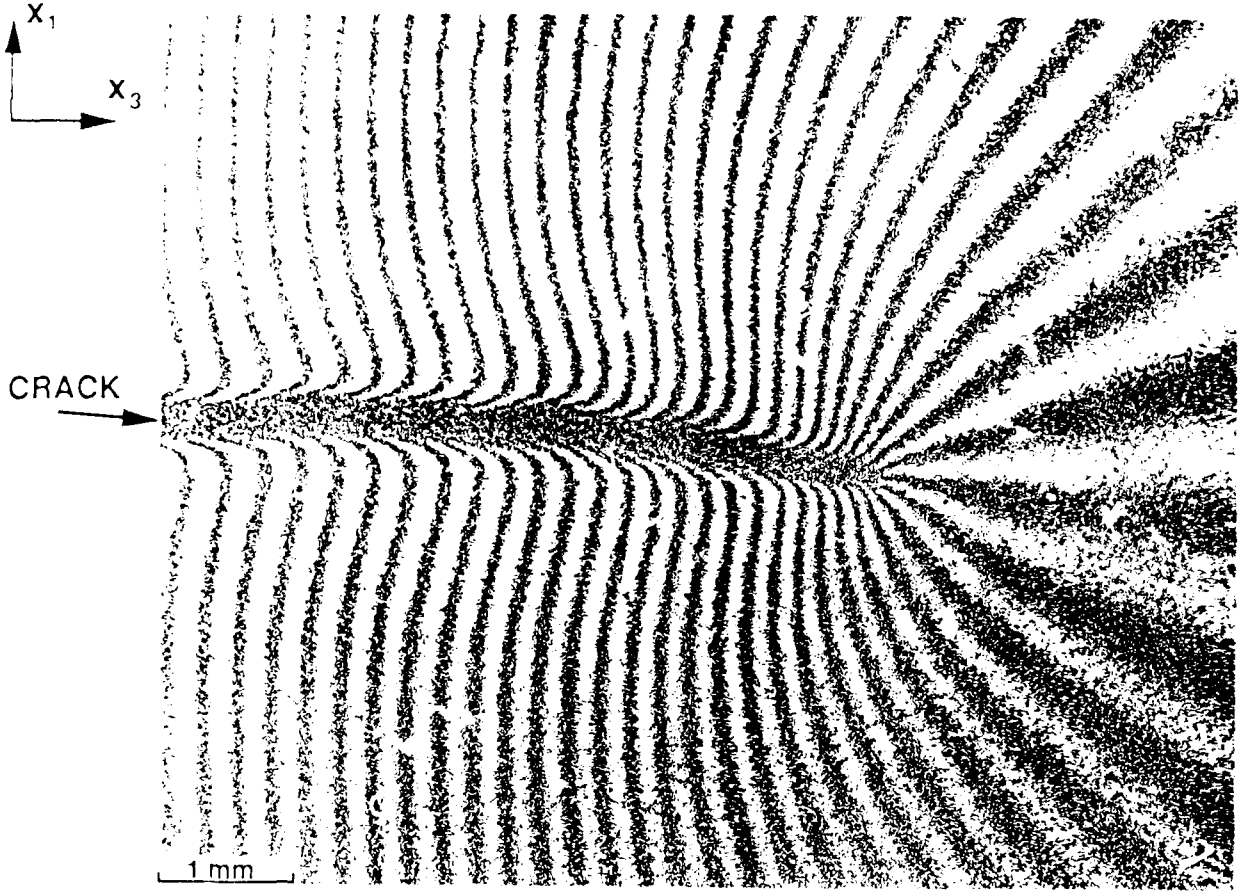
x_1
x_3
CRACK
1 mm

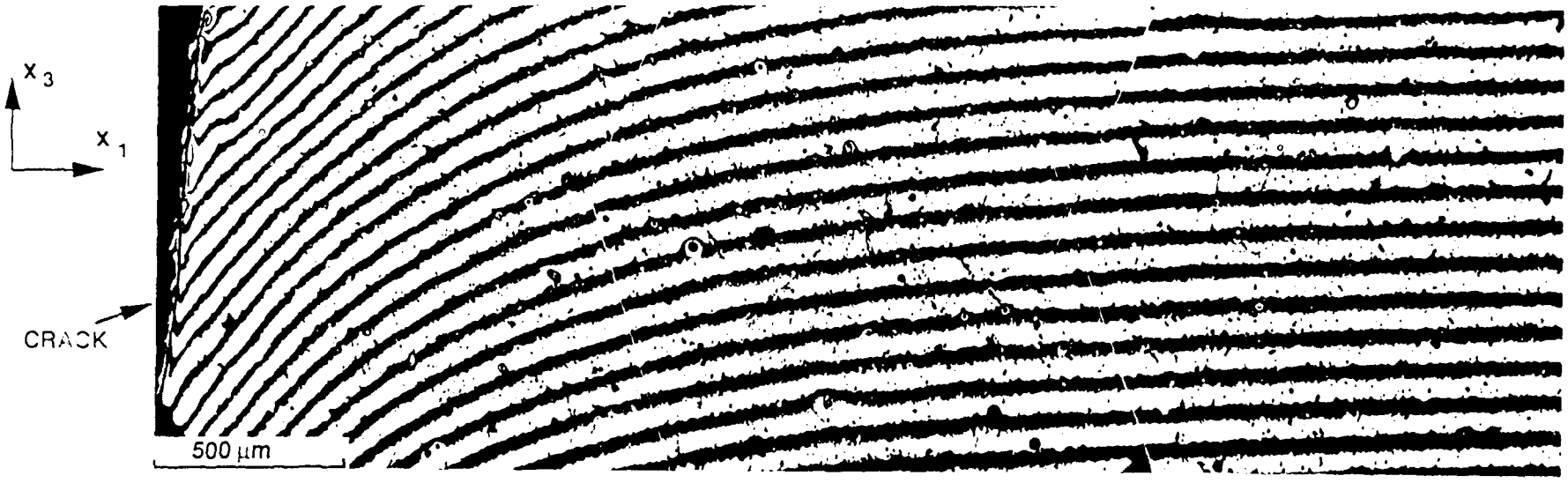
x_3
x_1
CRACK
500 μm

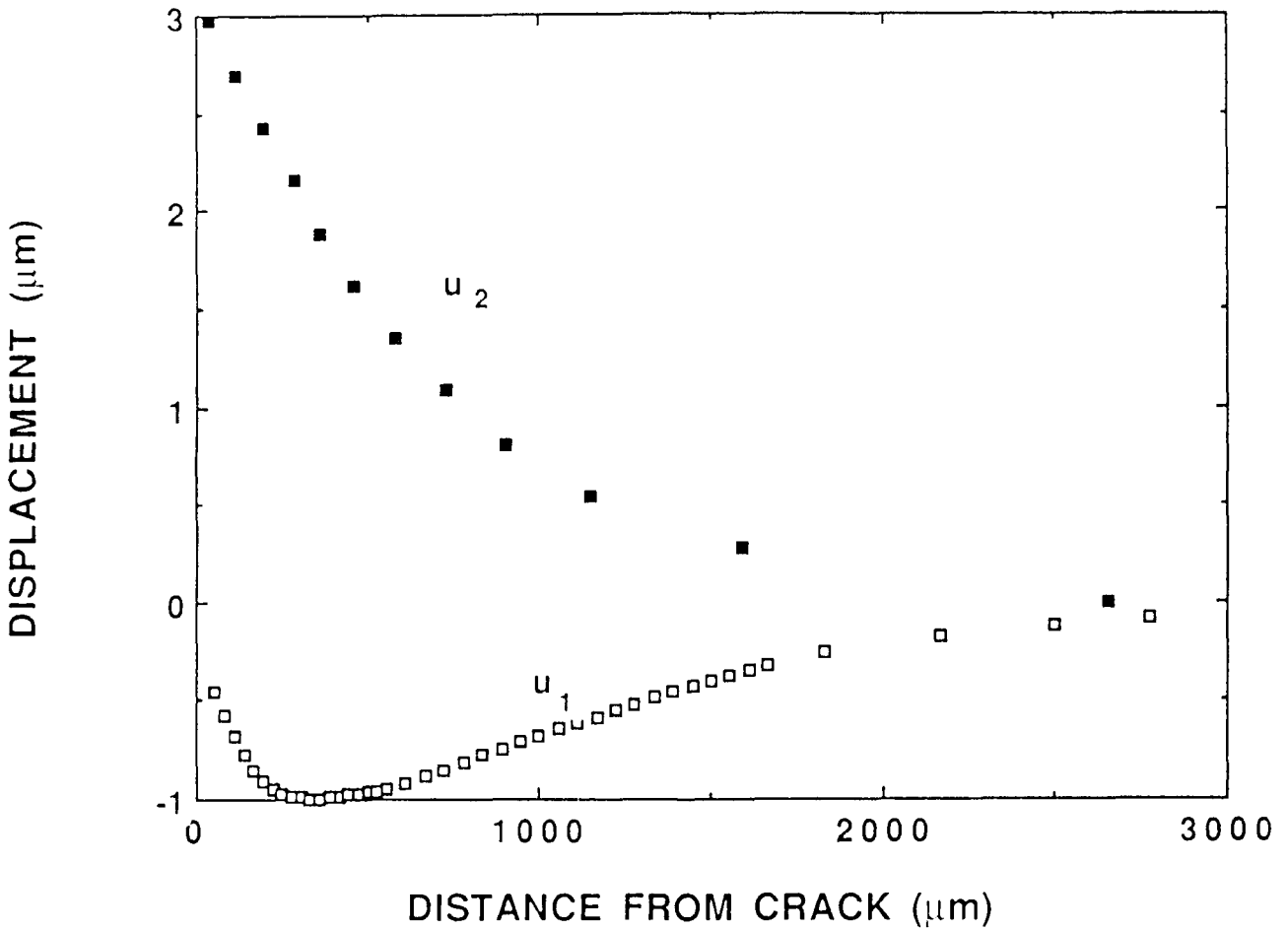
Data from "Moire Mg-PSZ"
DISPLACEMENT (μm)
3
2
1
0
-1
0
1000
2000
3000
DISTANCE FROM CRACK (μm)
u 2
u 1

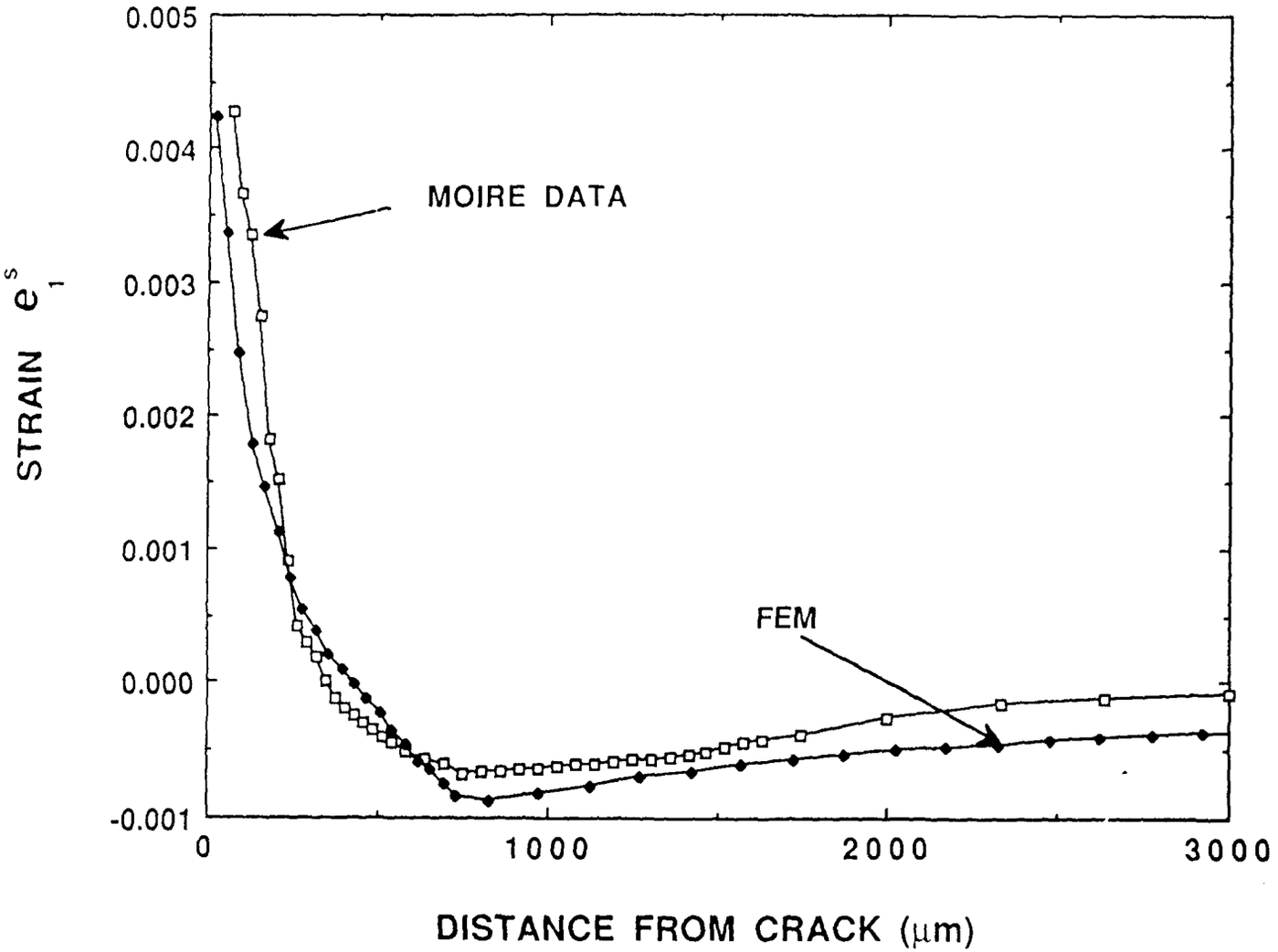
0.005
0.004
0.003
0.002
0.001
0.000
-0.001
STRAIN e_1^s
MOIRE DATA
FEM
0
1000
2000
3000
DISTANCE FROM CRACK (μm)

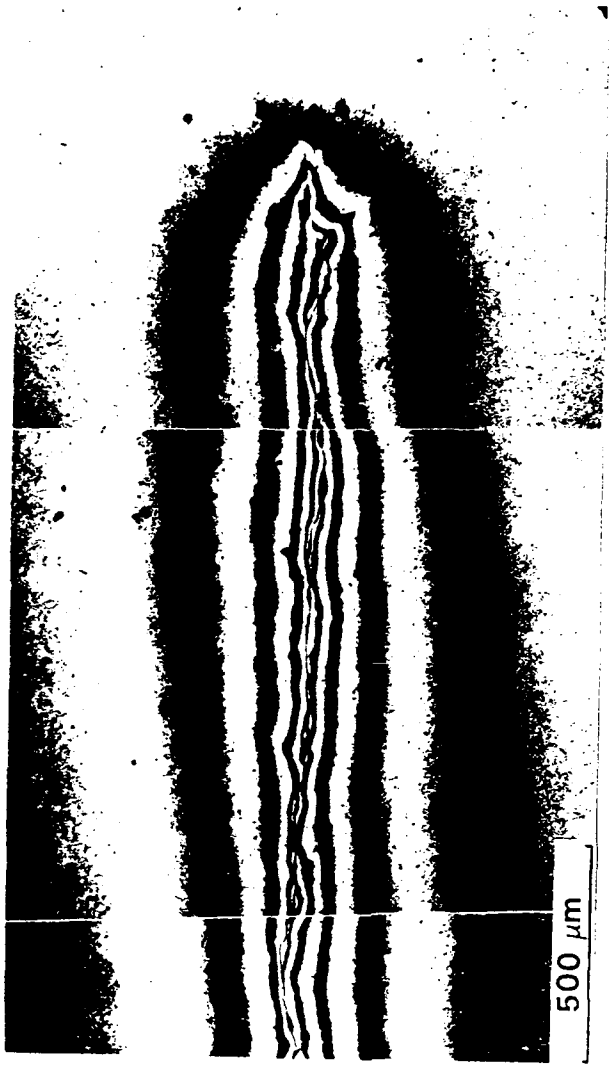
500 μm


100 μm
CRACK

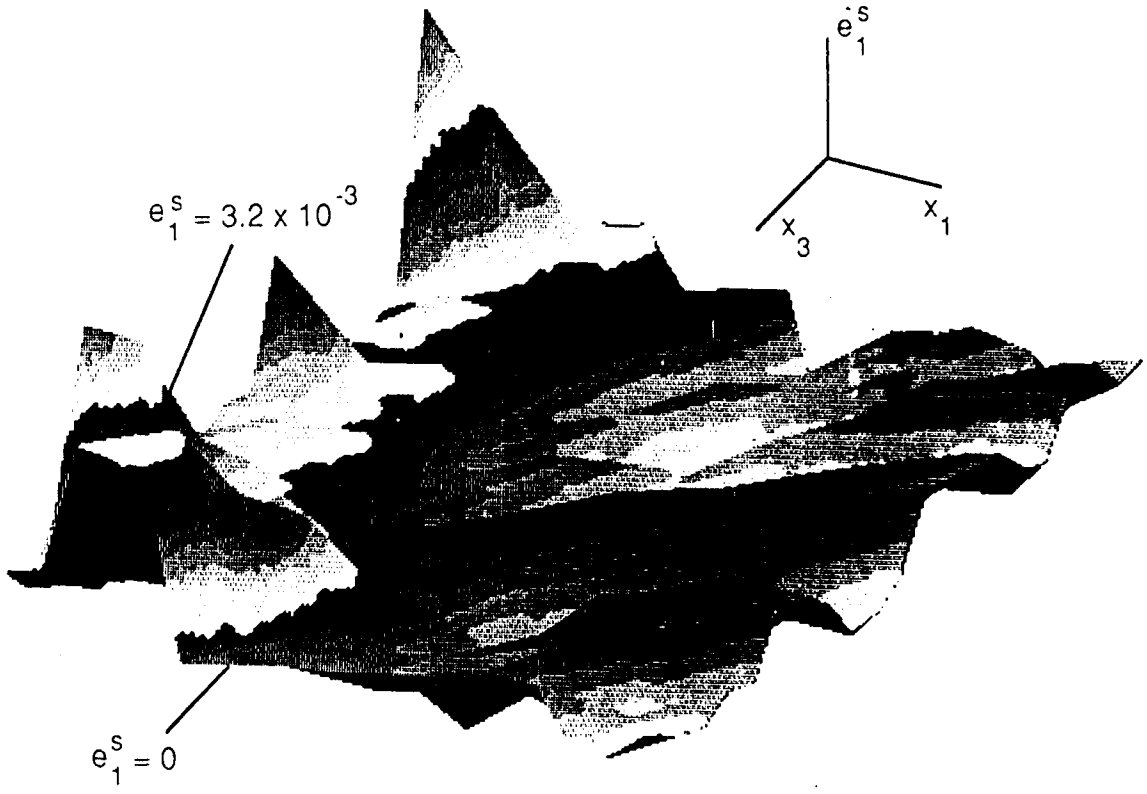
e_1^s
$e_1^s = 3.2 \times 10^{-3}$
x_3
x_1
$e_1^s = 0$

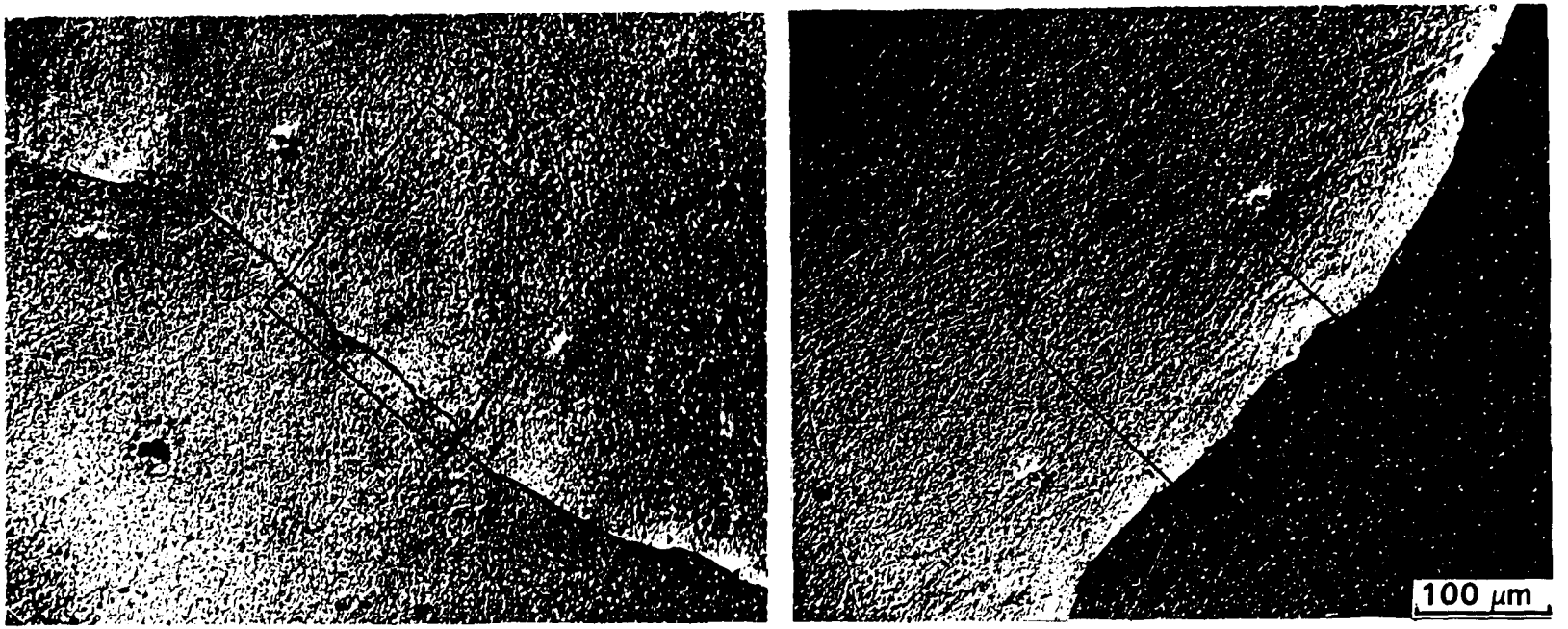
100 µm

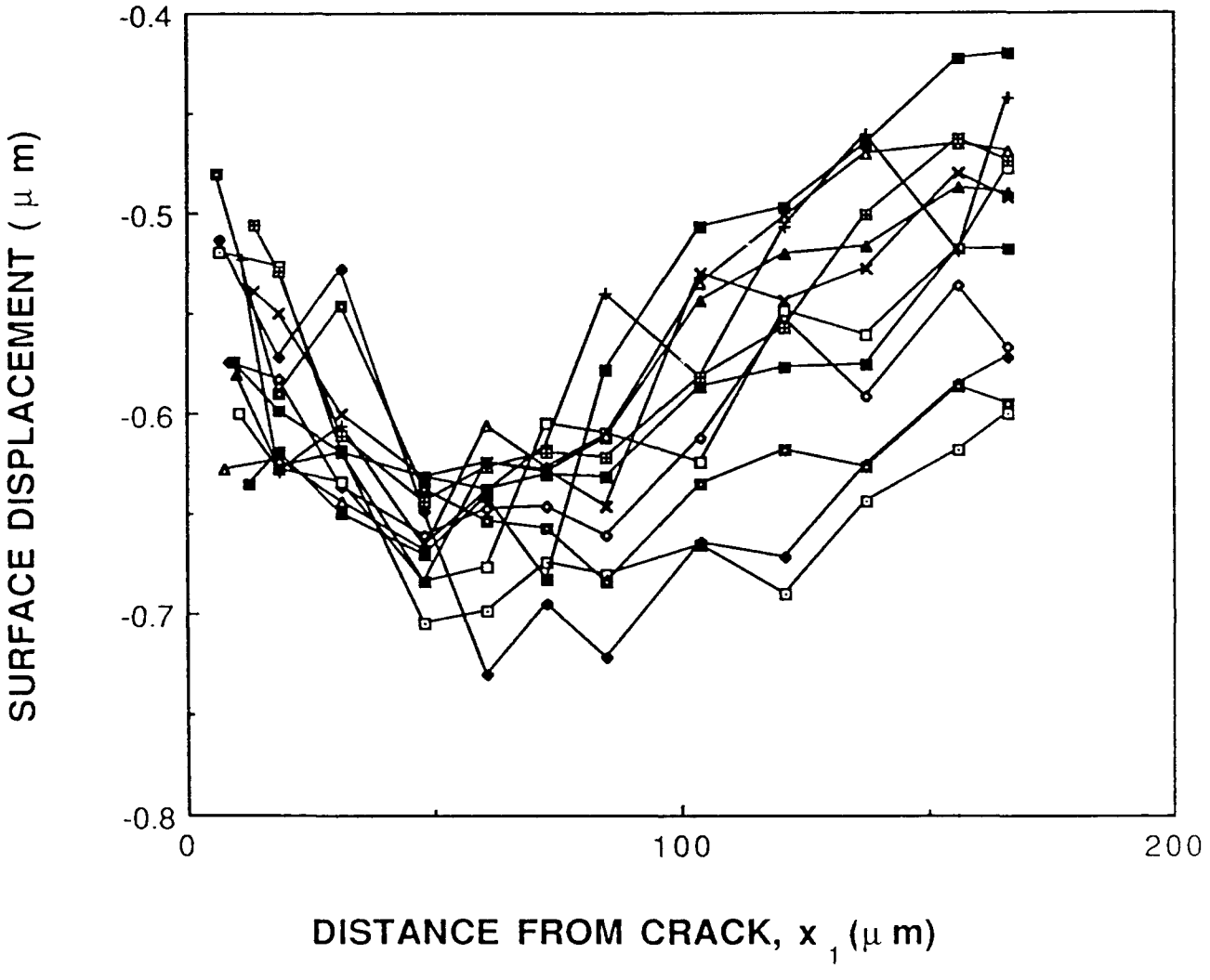
-0.4
-0.5
-0.6
-0.7
-0.8
0
100
200
SURFACE DISPLACEMENT (μ m)
DISTANCE FROM CRACK, x 1 (μ m)

7(A)

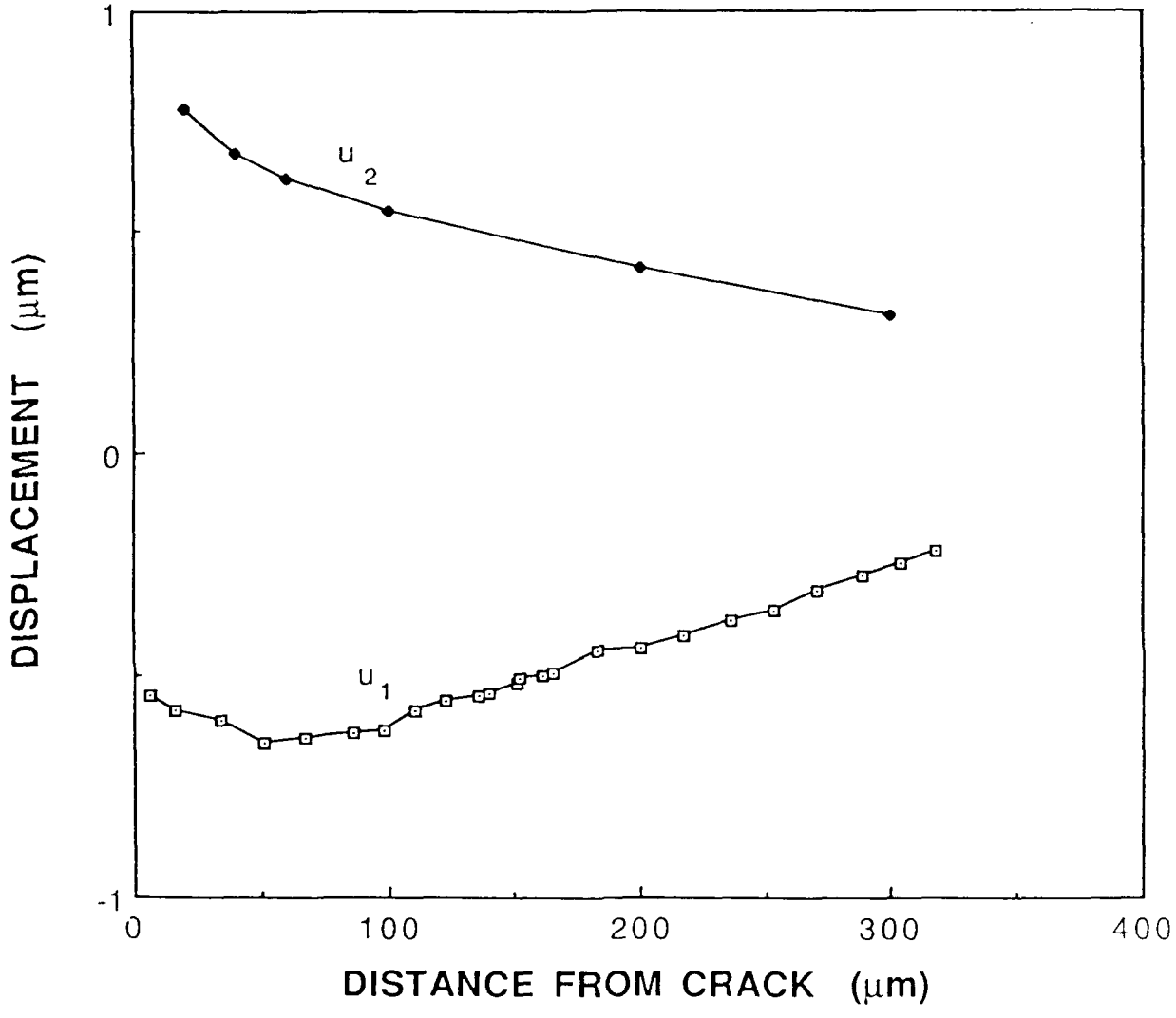
1
0
-1
0
100
200
300
400
DISPLACEMENT (μm)
DISTANCE FROM CRACK (μm)
u 2
u 1

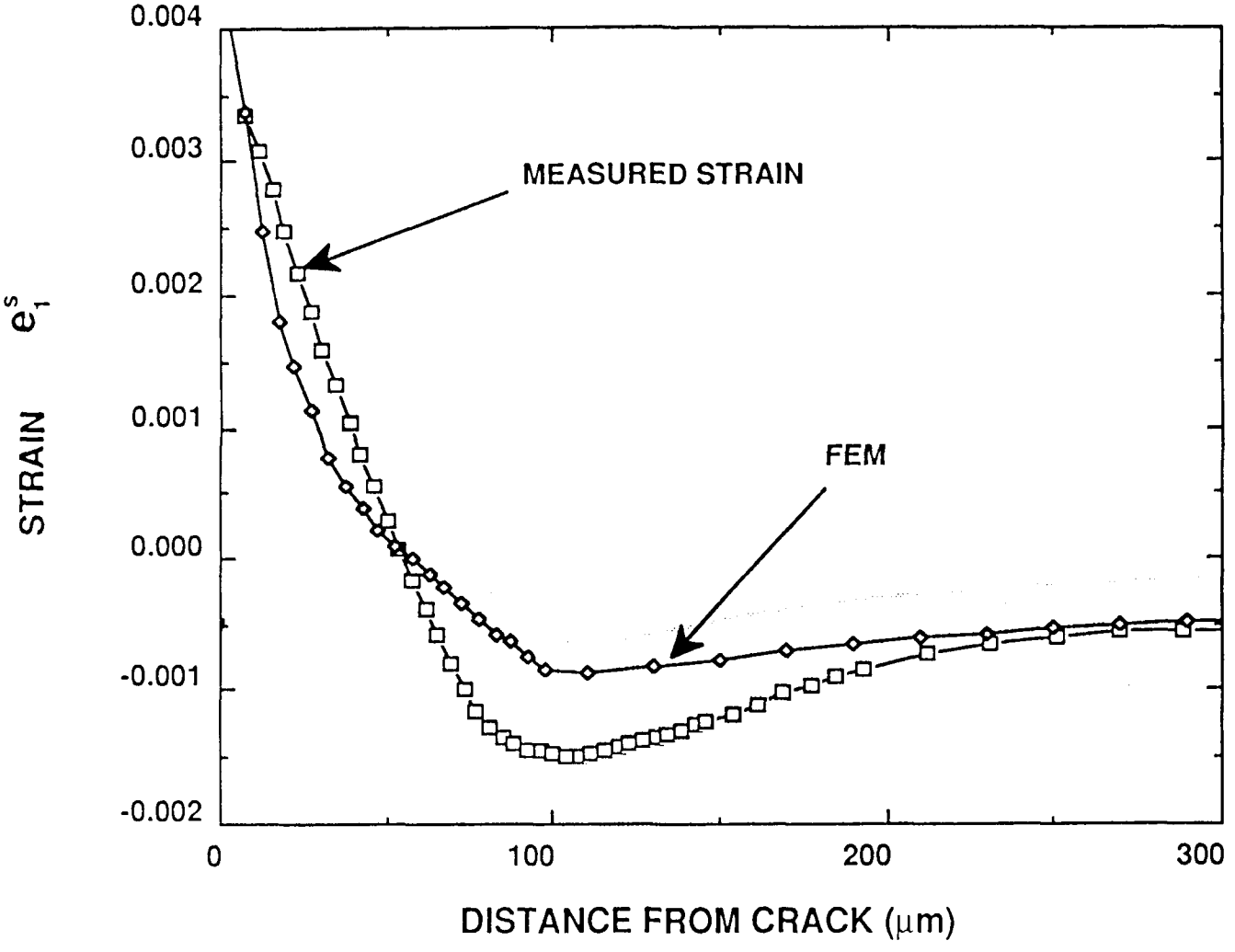
0.004
0.003
0.002
0.001
0.000
-0.001
-0.002
STRAIN e_1^s
MEASURED STRAIN
FEM
0
100
200
300
DISTANCE FROM CRACK (μm)

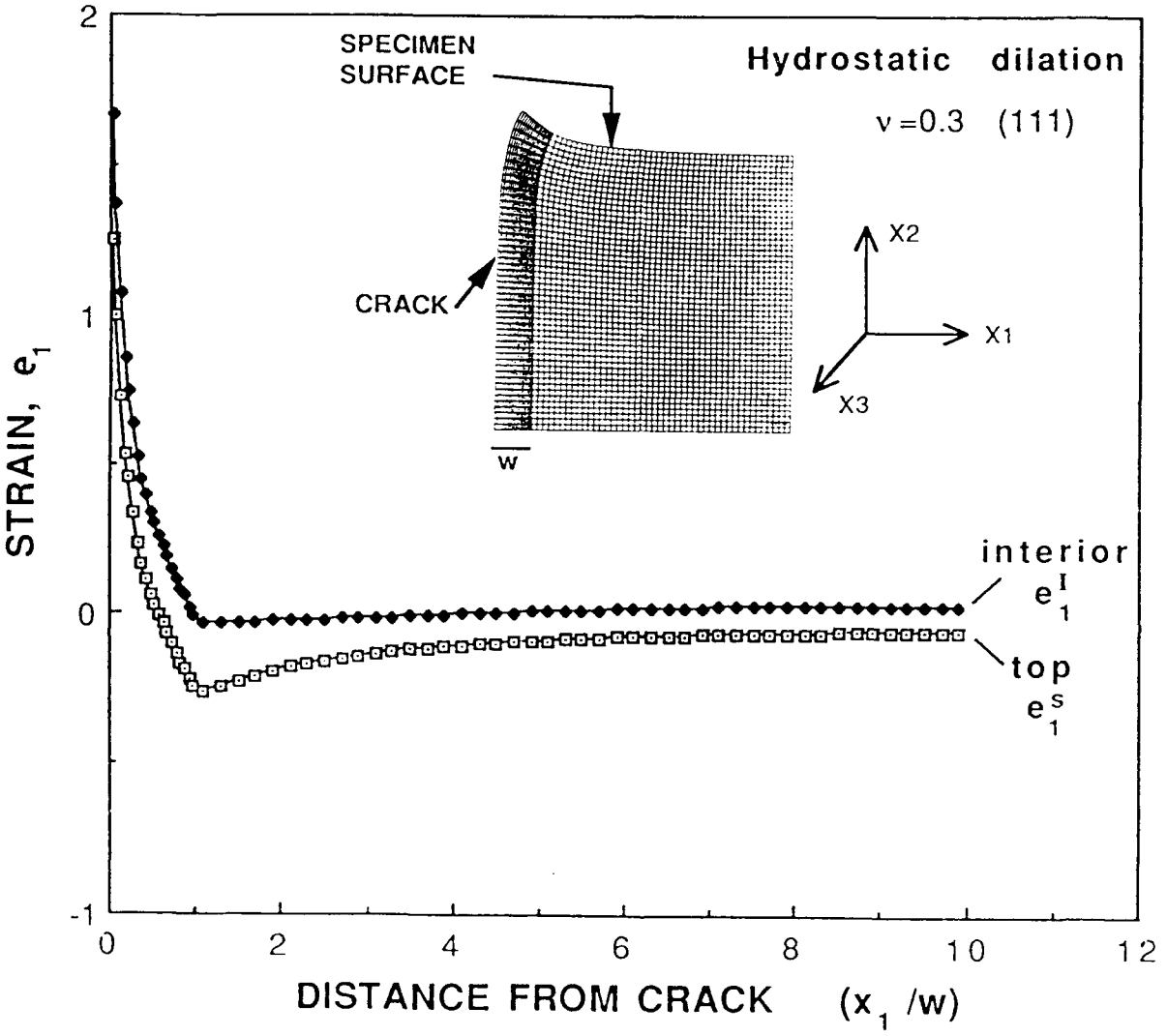
SPECIMEN
SURFACE
Hydrostatic dilation
ν =0.3 (111)
CRACK
X2
X1
X3
w
interior
e_1^I
top
e_1^s
STRAIN, e_1
2
1
0
-1
0
2
4
6
8
10
12
DISTANCE FROM CRACK (x_1 /w)

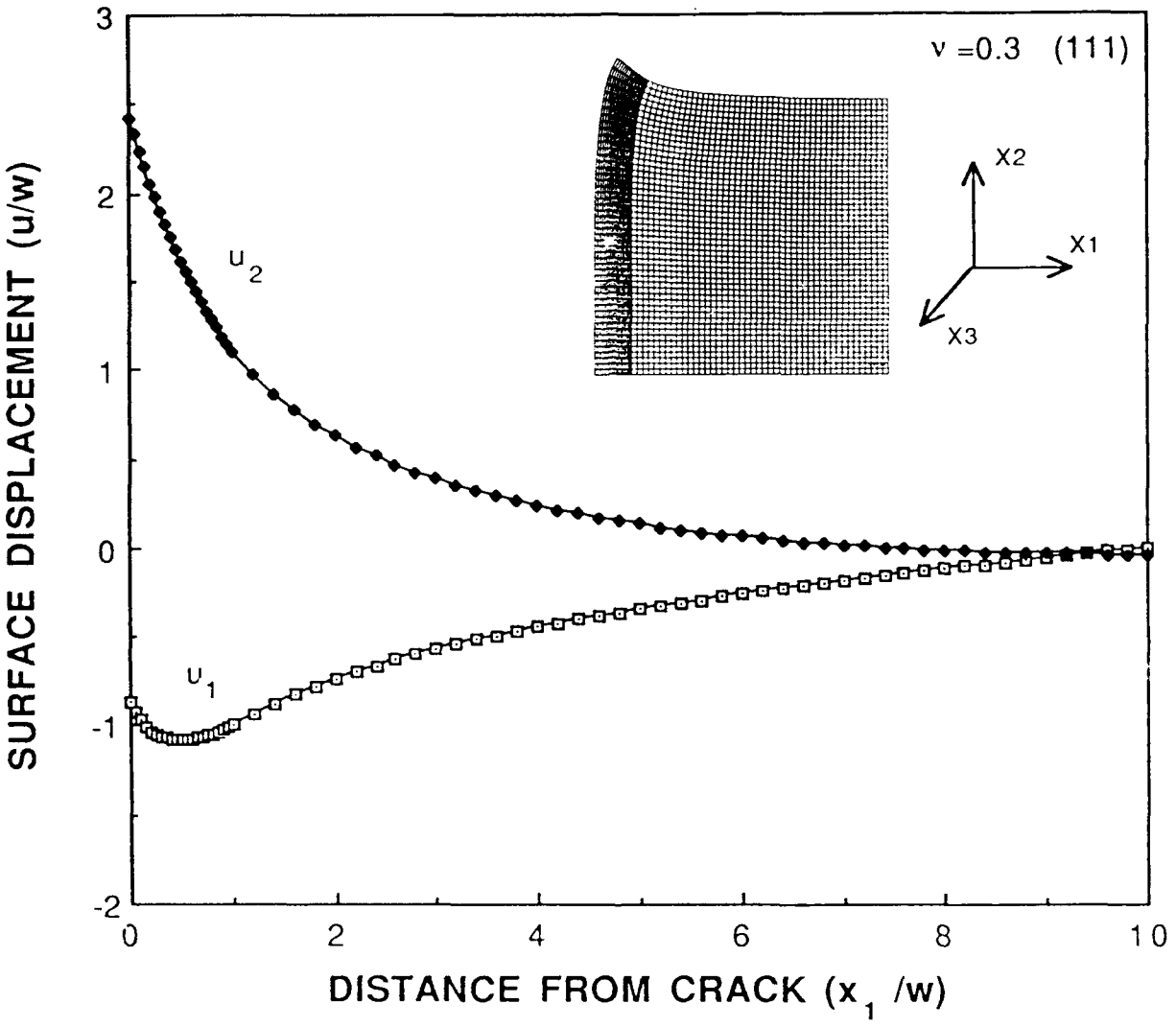
ν =0.3 (111)
X2
X1
X3
u_2
u_1
SURFACE DISPLACEMENT (u/w)
DISTANCE FROM CRACK (x_1 /w)
3
2
1
0
-1
-2
0
2
4
6
8
10

5(b)

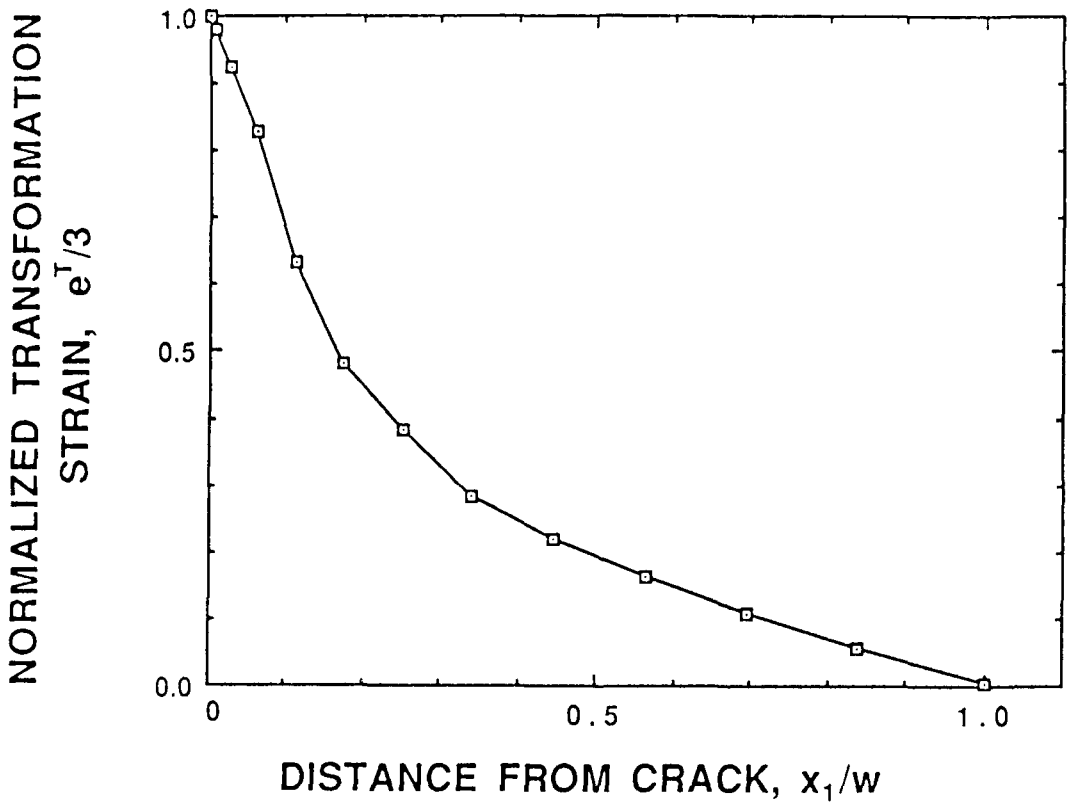
NORMALIZED TRANSFORMATION STRAIN, $e^T/3$
1.0
0.5
0.0
0
0.5
1.0
DISTANCE FROM CRACK, x_1/w

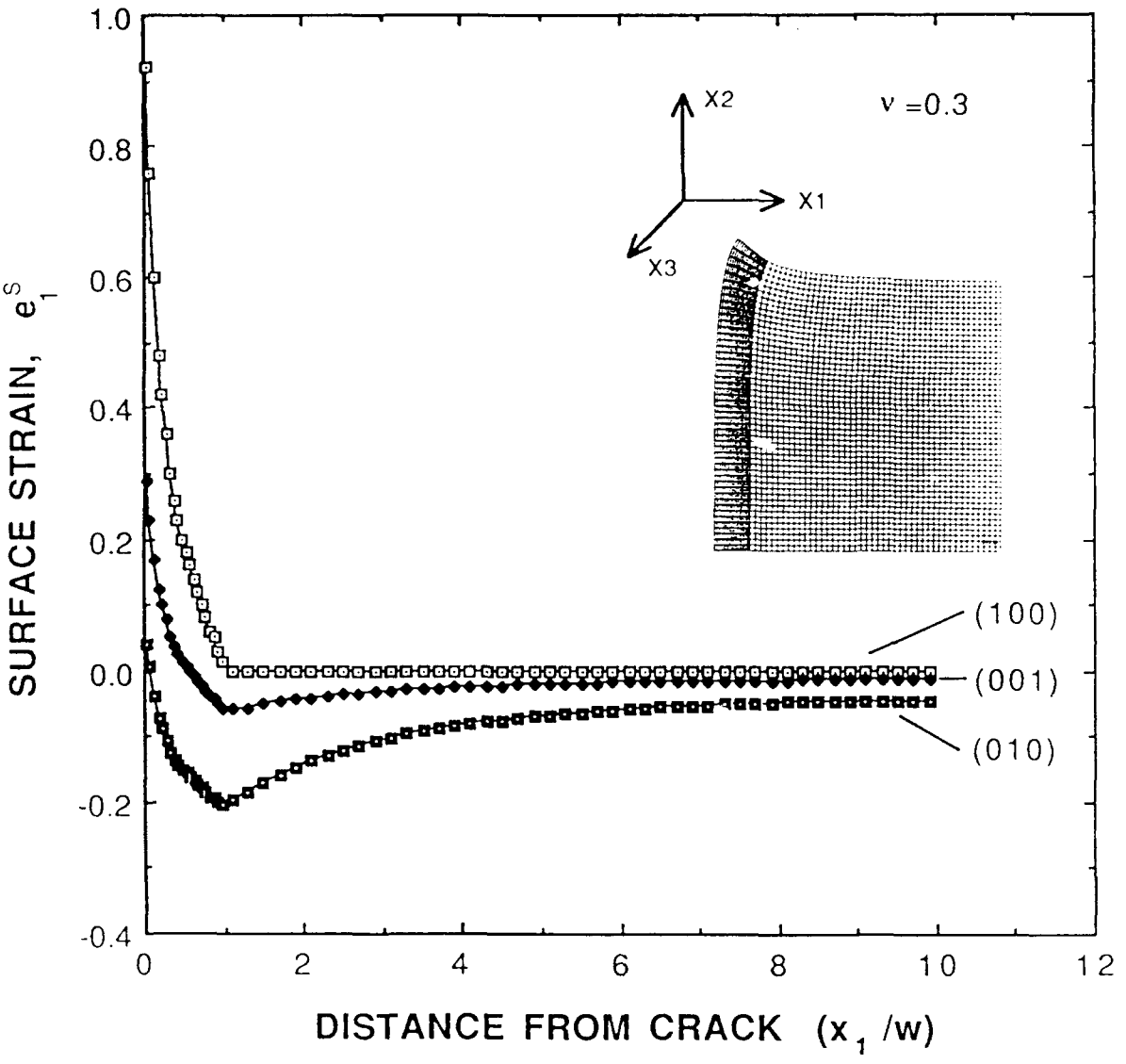
1.0
0.8
0.6
0.4
0.2
0.0
-0.2
-0.4
0
2
4
6
8
10
12
SURFACE STRAIN, e_1^S
DISTANCE FROM CRACK (x_1/w)
X2
X1
X3
ν =0.3
(100)
(001)
(010)

4.0 TRANSFORMATION RECOVERY IN Mg-PSZ AFTER HIGH TEMPERATURE ANNEALING

To be submitted to J. Am. Ceram. Soc.

RECOVERY OF CRACK TIP TRANSFORMATION ZONES IN ZIRCONIA AFTER HIGH TEMPERATURE ANNEALING

M.C. Shaw and D.B. Marshall
Rockwell International Science Center
1049 Camino Dos Rios
Thousand Oaks, CA 91360

A.H. Heuer and E. Enghels
Department of Materials Science and Engineering
Case Western Reserve University
Cleveland, OH 44106

ABSTRACT

Heat treatment in the temperature range 600-1000°C is known to restore the parent tetragonal phase within crack tip zones in Mg-PSZ that had previously undergone stress-induced martensitic transformation to the monoclinic phase. The stability of this reverse transformation during subsequent room temperature aging has been examined using Raman spectroscopy and surface displacement measurements. Partial transformation of material within the original zone back to the monoclinic phase was observed over periods of several months.

INTRODUCTION

Recent studies have shown that large residual crack openings are associated with the presence of transformation zones surrounding cracks in magnesia-partially-stablized zirconia.[1,2] The residual opening is thought to be a result of the dilatational strain associated with the martensitic tetragonal-to-monoclinic transformation which causes both wedging near the tip of the crack and bending of the arms of the test piece. The magnitude of the residual opening is dependent on the toughness of the material, the specimen geometry, and the size and growth history of the crack.[1] The opening is largest in high toughness materials and increases with crack extension, for a crack that begins with no transformation zone. Removal of the transformation zone by cutting along the crack with a saw blade eliminates the residual opening displacements, as does annealing in the temperature range 500 to 1000°C for periods as small as 20 min.

The last observation is consistent with the postulate that heat treatment in this temperature range causes reversal of the stress-induced tetragonal-to-monoclinic transformation. In this paper, we use several techniques to examine the stability, at ambient temperature, of such a zone that has undergone retransformation back to the tetragonal phase during heat treatments at 600 and 800°C. The reverse transformation is found not to be stable; over periods of months, the material within the original transformation zone transforms back to the monoclinic phase, giving almost complete recovery of the original residual displacement.

EXPERIMENTS

The material examined was a commercial 9 mole% magnesia-partially-stabilized zirconia* that had been heat treated at 1100°C for 20 min (subeutectoid aging[3,4]) to promote easy transformation and, thus, formation of large transformation zones surrounding cracks. The specimen geometry and loading conditions used to introduce cracks are described in detail elsewhere.[1,5] A "short DCB" specimen‡ was polished on one side and notched using a 100 μm thickness saw blade. After loading to form a stable crack, the specimen was annealed at 1000°C to convert any material that had transformed to monoclinic phase back to the tetragonal phase, then reloaded to grow the crack a further 4 mm. During reloading, the measured fracture resistance increased from an initial value of ~ 11 $MPa \cdot m^{1/2}$ to ~ 15 $MPa \cdot m^{1/2}$ after ~ 2 mm of crack extension, and remained constant thereafter.

The transformation zone was then characterized using several methods. The residual crack opening was measured at two locations, at the root of the notch and along the loading line 15 mm from the notch root. Raman spectroscopy[6-9] was used to measure the fracture of monoclinic phase as a function of distance from the crack plane at several locations behind the crack tip. From optical interference micrographs of the polished specimen surface, the out-of-plane displacements due to the transformation zone were measured in the region surrounding the crack.[9,10]

The specimen was then annealed at 600°C for 20 min. and the measurements were repeated 7 days after cooling. After ten days, the specimen was annealed at 800°C for 20 mins., and the measurements repeated 17 days later. These results indicated that

---

* Nilcra Ceramics Ltd., Northcote, Victoria, Australia, MS grade Mg-PSZ.
‡ Similar to a compact tension specimen, but with dimensions 30 mm × 25 mm.

recovery of the transformation zone had occurred. Therefore, to characterize the effect systematically, the specimen was annealed again at 800°C and the measurements were repeated at various intervals during the following 15 months.

RESULTS

Both Raman spectroscopy and measurements of surface uplift indicated that a transformation zone with dimensions approximately as shown in Fig. 1 surrounded the crack in its initial state. The zone width increased over the first 2 mm of crack growth, corresponding to the measured increase in crack resistance, and consistent with previous observations of zone development in nominally identical material.[9] Measurements of the fraction of monoclinic phase and the surface uplift along a line normal to the crack within the steady-state region, as indicated in Fig. 1, are shown in Fig. 2. These are also similar to previous observations.[9]

The variation of the crack opening displacement at the notch root during the sequence of room temperature aging and reannealing is shown in Fig. 3. After the first anneal at 600°C, the displacement was reduced from the initial value of 54 μm to 38 μm, consistent with results in Ref. 1. The specimen was then annealed at 800°C and left for 17 days at room temperature, whereupon the displacement had increased to 50 μm, close to its original value. Immediately after the second annealing at 800°C, the displacement was reduced to 29 μm. Measurements at regular intervals during room temperature aging over the next 17 months showed that the residual crack opening displacement completely recovered, the recovery being most rapid during the first several days.

Interference measurements of the surface uplift along the line O-Y normal to the steady-state crack of Fig. 1 are shown in Fig. 2(a), for several stages during the room

temperature aging. Corresponding measurements of the volume fraction of monoclinic phase by Raman spectroscopy are shown in Fig. 2(b). Both measurements indicated that most of the transformation zone was eliminated after annealing at 800°C, consistent with the observed reduction in residual crack opening. Moreover, both measurements showed that during subsequent room temperature aging, transformation from the tetragonal phase back to the monoclinic phase occurred spontaneously within the original transformation zone.

The results in Figs. 2 and 3 indicate a correlation between the recovery of the residual crack opening displacement and the retransformation of material within the original crack tip zone to the monoclinic phase. However, the magnitudes of the relative recovery of monoclinic phase and surface uplift are both much smaller than the relative recovery in crack opening. After 17 months, the displacement recovery was complete, whereas less than half of the original monoclinic phase adjacent to the crack was recovered and the zone width was less than half of its original value.

To test whether this apparent discrepancy arises because of differences in the transformation zone at the surface of the specimen and in the bulk, the specimen was sectioned and polished adjacent to the line marked in Fig. 1, along which the Raman and surface uplift measurements had been made. The Raman measurements were then repeated along lines on this new surface parallel to O-Y and corresponding to different depths in the original specimen. The resultant zone profiles were indistinguishable from that measured at the specimen surface.

DISCUSSION

The measurements of the previous section indicate that, whereas annealing of Mg-PSZ at 600 to 800°C causes reversal of the martensitic tetragonal-to-monoclinic transformation and thus removal of the transformation zone surrounding a crack, subsequent aging at room temperature without any applied stress causes partial recovery of the monoclinic phase within the original zone. This implies that remanent defects associated with the crack tip stresses, or with the stress-induced martensitic transformation, must remain after annealing in order to provide nucleation sites or driving forces for retransformation. Microcracks, which are known to accompany the transformation of tetragonal precipitates to monoclinic phase in this material, are a likely source of such defects.

The overall macroscopic shape change of the specimen, as characterized by the residual crack opening displacement, is similar to that of a two-way shape memory effect,[11,12] albeit with an activation barrier to the transformation that occurs after cooling. However, the crack opening displacement measurements alone do not necessarily imply a true shape memory effect (which requires recovery of shear strains[13]) in the material, since the observed displacement variations could be induced by purely hydrostatic transformation strains within the confines of the crack tip zone. However, complete recovery of the residual crack opening in this case would require complete recovery of the transformation within the zone, contrary to the observations from Raman spectroscopy and interference microscopy. Therefore, the shape strains associated with the initial stress-induced transformation appear to be different from those associated with the thermal transformation during subsequent annealing cycles.

ACKNOWLEDGEMENTS

Funding for this work was supplied by the U.S. Air Force Office of Scientific Research under Contract No. F49620-89-C-0031.

REFERENCES

1. R.W. Steinbrech, E. Inghels and A.H. Heuer, "Residual Displacement Effects during Crack Propagation Studies in High Toughness Magnesia-Partially-Stabilized Zirconia," J. Am. Ceram Soc. 73[7], 2016-2022 (1990).

2. S.J. Burns and M.V. Swain, "Fracture Toughness of MgO-Partially Stabilized ZrO_2 Specimen with K_R-Curve Behavior from Transformation Toughening," J. Am. Soc. 69[3], 226-30 (1986).

3. R.H.J. Hannink and M.V. Swain, "Magnesia-Partially Stabilizd Zirconia: The Influence of Heat Treatment on Thermomechanical Properties," J. Aust. Ceram. Soc. 18[2], 53-62 (1982).

4. M.J. Readey, A.H. Heuer and R.W. Steinbrech, "Annealing of Test Specimens of High-Toughness Magnesia-Partially Stabilized Zirconia," J. Am. Ceram. Soc. 71[1], C2-6 (1988).

5. A.H. Heuer, M.J. Readey and R. Steinbrech, "Resistance Curve Behavior of Supertough MgO-Partially-Stabilized ZrO_2," Mat. Sci. Eng. A105/106, 83-89 (1988).

6. D.R. Clark and F. Adar, "Measurement of the Crystallographically Transformed Zone Produced by Fracture in Ceramics Containing Tetragonal Zirconia," J. Am. Ceram. Soc. 65[6], 284-88 (1982).

7. R.H. Dauskardt, D.K. Veirs and R.O. Ritchie, "Spatially Resolved Raman Spectroscopy of Transformed Zones in MgO-Partially-Stabilized Zirconia," J. Am. Ceram. Soc. 72[7], 1124-30 (1989).

8. G. Katagiri, H. Isida, A. Ishitani, and T. Masaki, "Direct Determination of Transformation Zone Size in Y_2O_3 Containing Tetragonal ZrO_2 Polycrystals by Raman Microprobe," in Advances in Ceramics, Vol. 24, Science and Technology of Zirconia III, edited by S. Somiya and N. Yamamoto, Am. Ceram. Soc., Westerville, OH (1988).

9. D.B. Marshall, M.C. Shaw, R.H. Dauskardt, R.O. Ritchie, M. Readey and A.H. Heuer, "Crack Tip Transformation Zones in Toughened Zirconia," J. Am. Ceram. Soc. 73[9], 2659-66 (1990).

10. M.S. Dadkhah, D.B. Marshall, W.L. Morris and B.N. Cox, "Direct Measurement of Transformation Zone Strains in Toughened Zirconia," J. Am. Ceram. Soc., in press.

11. C.M. Wayman, "Martensitic Transformations: An Overview," pp. 1119-44, in Solid State Phase Transformations, eds., H.I. Aaronson, D.E. Laughlin, R.F. Sekerka and C.M. Wayman, Met. Soc. AIME 1982.

12. T. Saburi and S. Nenno, "The Shape Memory Effect and Related Phenomena," Ibid, pp. 1455-79.

13. P.E. Reys-Morel, J.-S. Cherng and I-Wey Chen, "Transformation Plasticity of CeO_2-Stabilized Zirconia Polycrystals: Pseudoelasticity and Shape Memory Effect," J. Am. Ceram Soc. 71[8], 648-57 (1988).

14. M.V. Swain, "Shape Memory Behavior in Partially Stabilized Zirconia Ceramics," Nature 322, 234-36 (1986).

FIGURE CAPTIONS

Fig. 1 Schematic diagram of (a) test specimen and (b) crack geometry showing dimensions and shape of transformation zone.

Fig. 2 (a) Out-of-plane surface displacements along the line OY in Fig. 1(b). Measurements from optical interference micrographs.

(b) Volume fraction of monoclinic phase along the line OY in Fig. 1(b). Measurements from Raman spectroscopy.

Fig. 3 Residual crack opening displacements measured at the root of the notch in Fig. 1 after various sequences of high temperature annealing and room temperature aging.

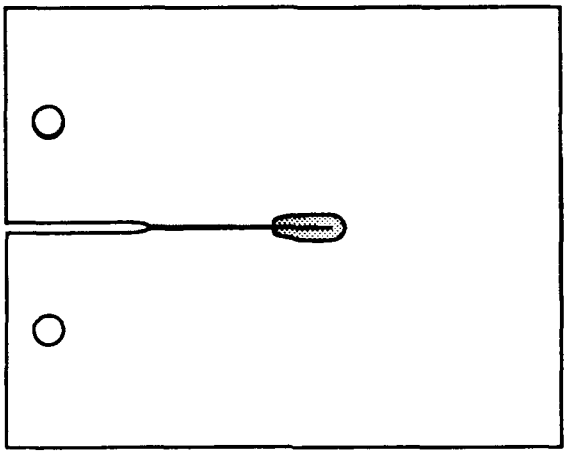

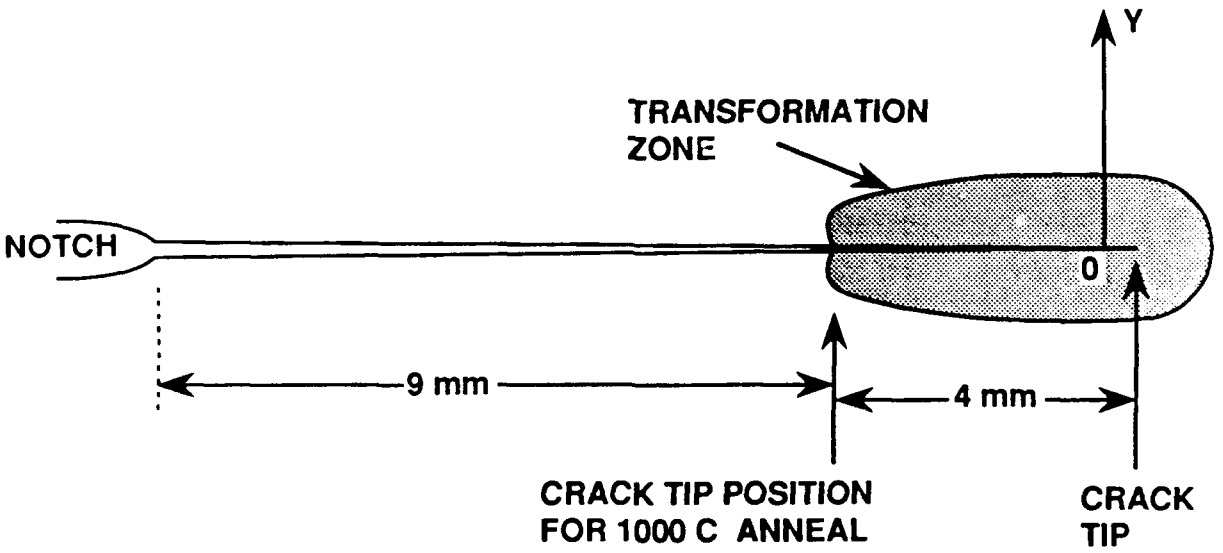
Y
TRANSFORMATION
ZONE
NOTCH
0
9 mm
4 mm
CRACK TIP POSITION
FOR 1000 C ANNEAL
CRACK
TIP

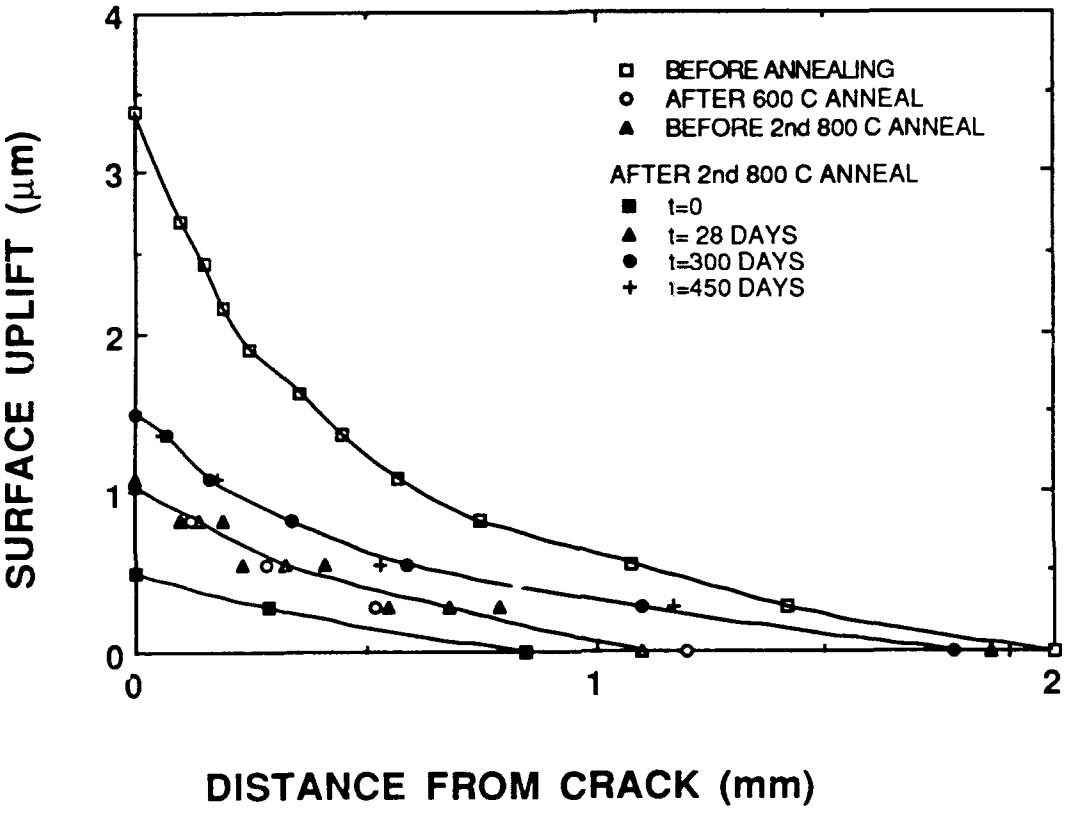
SURFACE UPLIFT (μm)
DISTANCE FROM CRACK (mm)
BEFORE ANNEALING
AFTER 600 C ANNEAL
BEFORE 2nd 800 C ANNEAL
AFTER 2nd 800 C ANNEAL
t=0
t= 28 DAYS
t=300 DAYS
t=450 DAYS
0
1
2
3
4

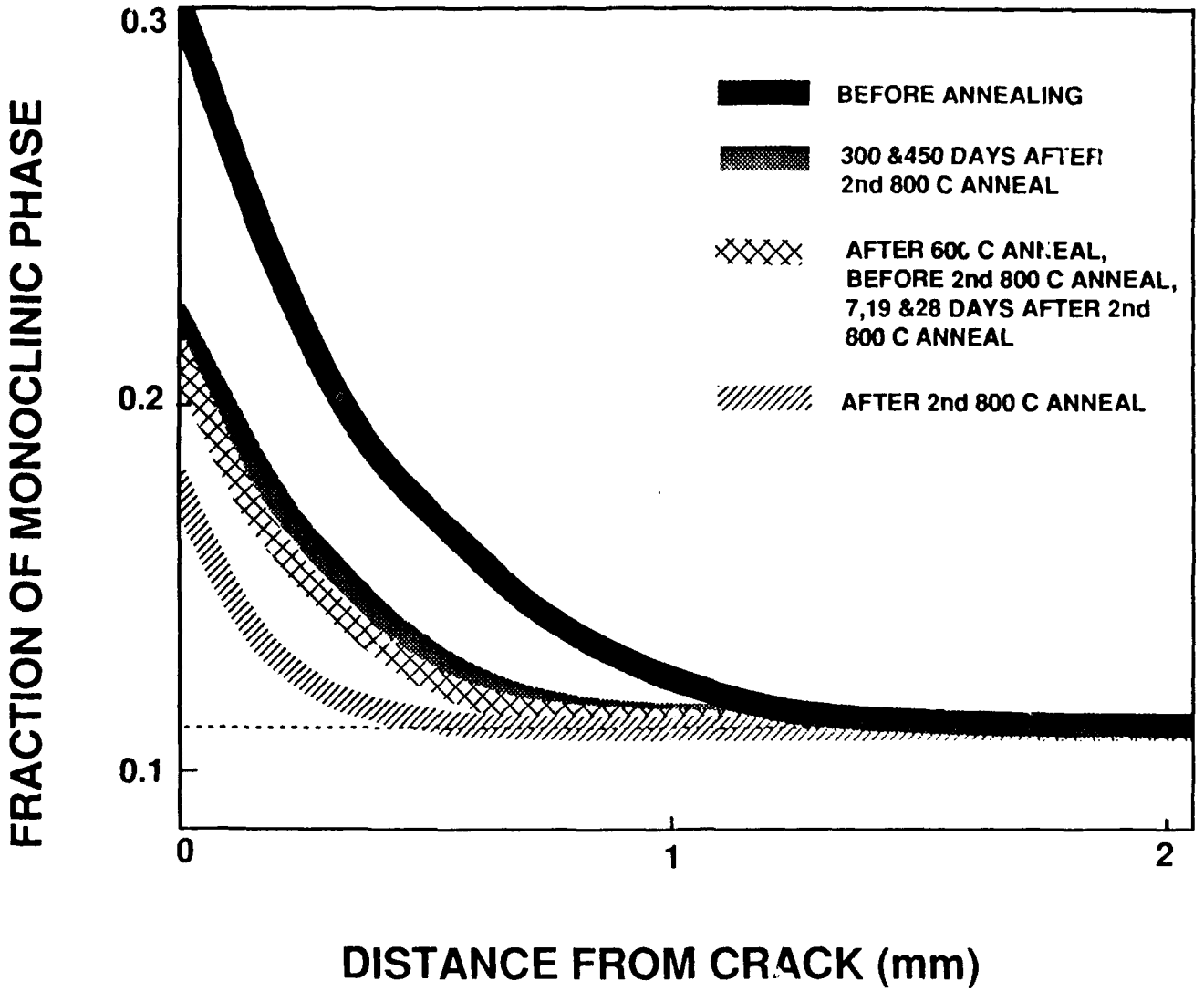
FRACTION OF MONOCLINIC PHASE
0.3
0.2
0.1
0
1
2
DISTANCE FROM CRACK (mm)
BEFORE ANNEALING
300 &450 DAYS AFTER 2nd 800 C ANNEAL
AFTER 600 C ANNEAL, BEFORE 2nd 800 C ANNEAL, 7,19 &28 DAYS AFTER 2nd 800 C ANNEAL
AFTER 2nd 800 C ANNEAL

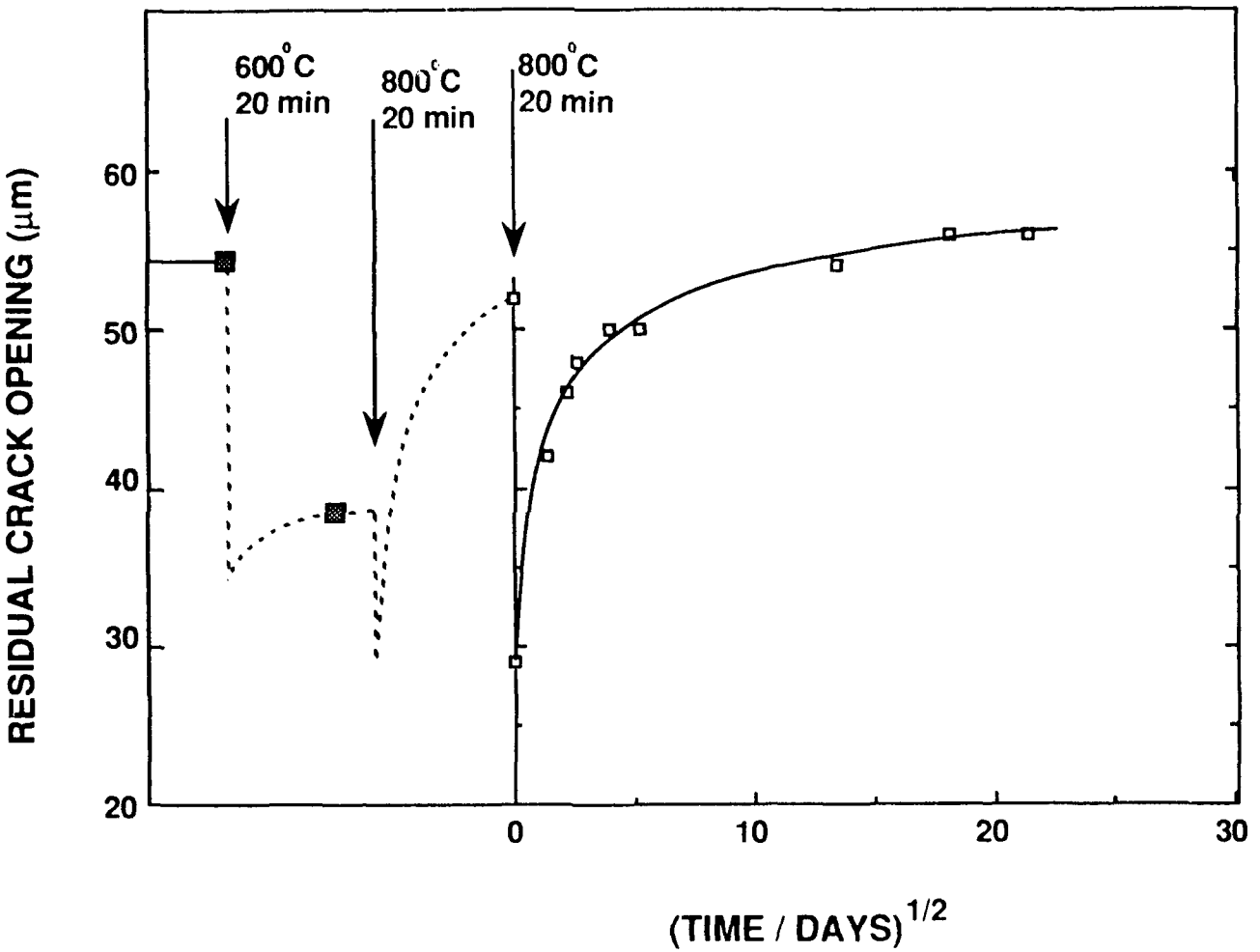
600°C
20 min
800°C
20 min
800°C
20 min
RESIDUAL CRACK OPENING (μm)
60
50
40
30
20
0
10
20
30
(TIME / DAYS)^1/2

5.0 CRACK SHIELDING IN CERIA-PARTIALLY STABILIZED ZIRCONIA

Published in J. Am. Ceram. Soc. 73(10), 3119-21 (1990).

journal

Reprinted from the Journal of the American Ceramic Society, Vol. 73, No. 10, October 1990

J. Am. Ceram. Soc., 73 [10] 3119-21 (1990)

Crack Shielding in Ceria-Partially-Stabilized Zirconia

David B. Marshall*

Rockwell International Science Center, Thousand Oaks, California 91360

The crack tip shielding stress intensity factor has been calculated for several elongated transformation zone shapes observed in high-toughness ceria–zirconia ceramics. The results show that the measured increases in fracture toughness of these materials are consistent with the crack tip shielding mechanism, to which the toughening of other zirconia ceramics has been attributed. Moreover, the presence of a very elongated zone ahead of a steady-state crack is shown to decrease the degree of shielding compared with that of a zone with semicircular frontal shape and equivalent width by a factor of about 2. [Key words: fracture toughness, tetragonal zirconia polycrystals, cerium, shielding, transformations.]

I. Introduction

Several recent studies have demonstrated that high fracture toughnesses, in the range 12 to 20 MPa·m$^{1/2}$, can be achieved in ceria-partially-stabilized zirconia (Ce-TZP) ceramics that readily undergo martensitic transformation from tetragonal to monoclinic phase.[1-7] However, the shapes of the transformation zones surrounding cracks in these materials are very different from those in other zirconia materials of comparable toughness; in magnesia-partially-stabilized zirconia (Mg-PSZ) the zone extends approximately equal distances ahead and to the side of the crack,[9] whereas the zone in Ce-TZP is very elongated, extending ahead of the crack a distance ~10 to 20 times the zone width (Fig. 1).[1-4] This appearance of a slitlike zone ahead of the crack has prompted several analyses of crack growth and toughening in terms of a Dugdale zone model.[3,4] Moreover, in one of these studies[4] it was specifically suggested that the crack tip shielding mechanism, which is generally accepted as the source of toughening in other toughened zirconia materials, is not applicable for Ce-TZP.

Calculations of the crack tip shielding due to transformation zones with the shapes observed in Ce-TZP are presented here, with two purposes in mind. One is to determine whether such shielding is indeed consistent with the measured fracture toughness. The other is to assess whether a substantial increase in toughness might be possible by modifying the microstructure to eliminate or reduce the extended frontal zone. The large frontal zone is detrimental to toughening by crack tip shielding, since dilatational transformation of material located within an angular range of ±60° ahead of the crack causes an increase in crack tip stresses.[10,11]

II. Analysis

Crack tip shielding occurs when the transformation strains within the zone surrounding the crack act to reduce the stress intensity factor near the crack tip, as characterized by

$$K_{tip} = K_a + K_s \tag{1}$$

where K_a is the applied stress intensity factor and K_s is the shielding stress intensity factor due to the zone. The condition for crack growth is taken as $K_{tip} = K_0$, the fracture toughness of the fully transformed material, whereupon $-K_s$ is the increase in fracture toughness due to the transformation zone. The magnitude of K_s can be calculated following the method of McMeeking and Evans,[10] by applying imaginary surface tractions to the boundary of the transformation zone to restore the original shape that it had before transformation, and applying a weight function method to compute the stress intensity factor due to the body forces, **T**, needed to cancel these tractions:

$$K_s = \int_\Gamma \mathbf{T} \cdot \mathbf{h}\, ds \tag{2}$$

where ds is an element of the zone boundary Γ, ν is Poisson's ratio, and **h** is the weight function, given, for mode I loading in an isotropic homogeneous body in plane strain, by[10]

$$\begin{Bmatrix} h_1 \\ h_2 \end{Bmatrix} = \frac{1}{2\sqrt{2\pi}(1-\nu)\sqrt{r}} \times \begin{Bmatrix} \cos(\theta/2)[2\nu - 1 + \sin\theta/2 \sin 3\theta/2] \\ \sin(\theta/2)[2 - 2\nu - \cos\theta/2 \cos 3\theta/2] \end{Bmatrix} \tag{3}$$

where r and θ are position coordinates relative to the crack tip.

To assess the role of the extended frontal zone on crack tip shielding, Eq. (2) was evaluated for the steady-state (i.e., constant zone width in wake of crack) zones shown in Fig. 1, as depicted by Rose and Swain.[3] The net transformation strain within the zone was taken to be hydrostatic dilatation, so that the tractions **T** consist of outward acting pressure P normal to the zone boundary (including the crack surfaces) as shown in Fig. 1(B). The pressure is related to the unconstrained trans-

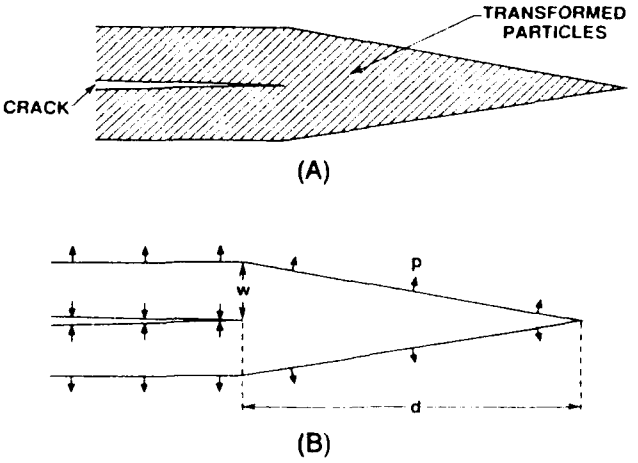

Fig. 1. (A) Steady-state transformation zone shape in Ce-TZP (from Ref. 3). (B) Zone boundary and tractions used for shielding calculations of Fig. 2.

I-W. Chen—contributing editor

Manuscript No. 197553. Received May 24, 1990; approved August 1, 1990.
Supported by the U.S. Air Force Office of Scientific Research under Contract No. F49620-89-C-0031.
*Member, American Ceramic Society

formation strain e^T and the volume fraction, f, of material transformed within the zone by[10]

$$p = fe^T E/3(1 - 2\nu) \quad (4)$$

where E is Young's modulus. Evaluation of Eq. (2) for the zone configuration of Fig. 1(B), with various ratios of length, d, to width, w, gives the result

$$K_s(1 - \nu)/e^T Ef\sqrt{w} = \kappa(d/w) \quad (5)$$

where the function $\kappa(d/w)$ is plotted in Fig. 2. At $d/w = 0$ (i.e., no frontal zone) the value $\kappa(d/w) = -0.37$ is the same as the corresponding result given by McMeeking and Evans[10] as an upper bound for the toughening. As the frontal zone gets very large ($d/w \to \infty$) K_s approaches zero, but it does so very slowly ($\kappa = -0.033$ at $d/w = 1000$ and $\kappa = -0.0033$ at $d/w = 10^5$).

Also shown in Fig. 2 are results from McMeeking and Evans[10] for steady-state zones with two other frontal zone shapes, one defined by a semicircle centered on the crack tip and the other defined by a contour of constant hydrostatic stress in the prior elastic crack-tip field. The semicircular shape is characteristic of zones in high-toughness Mg-PSZ materials.[9] The results in Fig. 2 indicate that replacement of the long frontal zone with $d/w \sim 20$ in Ce-TZP by a semicircular frontal zone would more than double the toughening due to transformation shielding.

To ascertain whether the measured fracture toughness of Ce-TZP is consistent with a shielding mechanism, K_s was calculated for two transformation zones from the paper by Yu and Shetty,[4] who also measured the parameters needed to calculate the shielding. The zone boundaries, corresponding to two stages of growth of a crack which initially did not have a zone, are shown in Fig. 3(A): the zone that developed after 180 μm of crack extension, at $K_a = 9.9$ MPa·m$^{1/2}$, was traced directly from Fig. 2 of Ref. 4, whereas the zone corresponding to 1.3 mm of crack extension (broken lines) at $K_a = 14.5$ MPa·m$^{1/2}$ was drawn to be consistent with the dimensions $w = 340$ μm and $d/w = 13$ given in Ref. 4. An estimate of the shielding stress intensity factor for the larger zone, using the result from McMeeking and Evans[10] for a steady-state crack with a frontal zone defined by a hydrostatic stress contour (i.e., $\kappa = 0.22$ in Eq. (5)), gave $K_s = 45$ MPa·m$^{1/2}$, much larger than the measured fracture toughness.[4] However, the observed zone shapes of Fig. 3(A) differ from the shape corresponding to this result, both in their

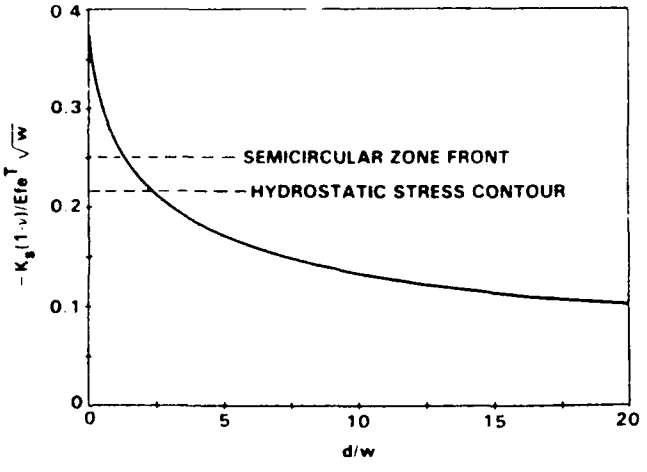

Fig. 2. Crack tip shielding stress intensity factors for steady-state cracks. Solid curve refers to zones with the shape depicted in Fig. 1(B) with various relative zone dimensions, d/w, ahead of the crack. Results for zones defined ahead of the crack by a semicircle and by a contour of constant hydrostatic stress in an elastic crack tip field are also shown.

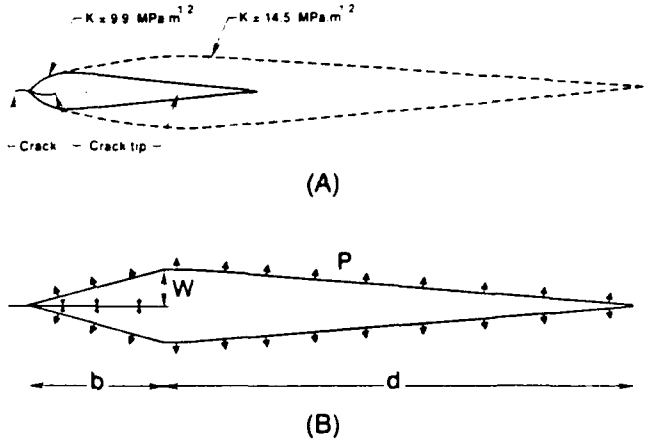

Fig. 3. (A) Transformation zone boundaries corresponding to two stages of crack growth (from data in Ref. 4): solid lines at crack extension of 180 μm, broken lines at crack extension of 1.3 mm. (B) Zone shape and tractions used to calculate K_s for the zones of (A).

form ahead of the crack tip and in the absence of fully developed steady-state wake regions. To evaluate K_s for the zones of Fig. 3(A), the shapes were approximated as in Fig. 3(B), with $b/w = 2$ for the smaller zone and $b/w = 4$ for the larger zone. The net transformation strain was assumed to be hydrostatic dilation. With these assumptions, the boundary tractions are defined by Eq. (4), as in the above calculation, and evaluation of Eq. (2) gives $\kappa = -0.043$ and $\kappa = -0.070$ for the smaller and larger zones. The corresponding values of K_s (with $f = 0.8$ from Ref. 4, $E = 200$ GPa, $\nu = 0.25$, and $e^T = 0.04$) are -4.7 MPa·m$^{1/2}$ for the smaller zone ($w = 166$ μm) and -11 MPa·m$^{1/2}$ for the larger zone ($w = 340$ μm). These values of K_s should be regarded only as estimates, since the value of f was obtained by X-ray diffraction from the fracture surface and was assumed to be constant throughout the zone, whereas the fraction of material transformed usually decreases with distance from the crack.[9] Also, possible effects of a net shear component in the transformation zone or of microcracks that have been observed within the zone[3] have not been considered. Nevertheless, the values of K_s are consistent with the measured values of K_a (9.9 and 14.5 MPa·m$^{1/2}$), in the sense that the magnitude of K_s is smaller than, but a substantial fraction of, K_a: Eq. (1) with these two values of K_s gives $K_0 = 5.2$ and 3.5 MPa·m$^{1/2}$ for the toughness of the fully transformed material.

In view of these results, it is worthwhile contemplating microstructural changes that might lead to a reduced frontal zone and consequential increase in toughness. The reason for the formation of the elongated frontal zone is not known, but it is thought to be associated with a strong tendency to autocatalytic transformation. Effects of autocatalytic transformation in Ce-TZP have been observed in many other experiments. These include sudden bursts of transformation that occur upon cooling through the M_s temperature, as well as load drops that occur during tensile loading experiments, coinciding with the formation of narrow, well-defined bands of transformed material oriented normal to the applied tension.[5]

A possible approach for controlling the autocatalytic transformation may be suggested by comparing the behaviors and microstructures of Ce-TZP and high-toughness Mg-PSZ. In Mg-PSZ the transformation zone ahead of a crack is approximately semicircular.[9] Mg-PSZ also undergoes autocatalytic transformation, as seen by well-defined bands on the surfaces of specimens loaded in either tension or compression.[12,13] However, rather than extending completely through the specimen, the bands arrest at grain boundaries. Because the bands are arrested, separate initiation of the transformation

at multiple locations is necessary, resulting in a smoothly increasing stress–strain curve and progressive transformation when cooling through the M_s temperature. Such arrest of transformation bands presumably also modifies the shape of the transformation zone ahead of a crack tip. The essential microstructural difference between the magnesia- and ceria-doped materials is that the Mg-PSZ contains a dual-scale microstructure, with small tetragonal precipitates (lens-shaped with largest diameter ~300 nm) within large grains (~50 μm in diameter) of cubic phase, whereas the Ce-TZP consists simply of a polycrystalline array of tetragonal grains of uniform size (several micrometers) without any barriers to arrest a band of autocatalytically transforming grains once it forms. Tsai, Yu, and Shetty[14] have shown that the presence of second-phase Al_2O_3 grains of similar size and spacing as the ZrO_2 grains is effective in preventing the autocatalytic transformation and in modifying the shape of the zone, but also leads to reduced zone width. By analogy with Mg-PSZ, if a dual-scale microstructure could be created in Ce-TZP, with barriers distributed on a scale substantially larger than the grain size, it may be possible to eliminate the large crack tip frontal zone while maintaining the width of the wake zone and thereby increase the fracture toughness by approximately a factor of 2. Several approaches are being pursued to test this hypothesis, including introduction of large platelets of Al_2O_3 and fabrication of layered structures.

III. Conclusion

In conclusion, the calculated shielding stress intensity factors confirm that the measured fracture toughness in Ce-TZP is consistent with the toughening being due to crack shielding from the observed transformation zones. Although this does not rule out the possibility of a Dugdale zone model as proposed in Refs. 3 and 4, we note that the shielding mechanism is also consistent with the reported[4] linear dependence of the zone width on the square of the applied stress intensity factor.[9] According to the crack shielding model, microstructural modifications that decrease the elongation of the zone ahead of the crack could increase the toughness by a factor of approximately 2.

References

[1]M. V. Swain, R. H. J. Hannink, and J. Drennan, "Some Interfacial Related Properties of Transformation Toughened Ceramics", p. 819 in Ceramic Microstructures '86, Role of Interfaces. Edited by J. A. Pask and A. G. Evans. Plenum Press, New York, 1987.

[2]R. H. J. Hannink and M. V. Swain, "Metastability of Martensitic Transformation in a 12 mol% Ceria–Zirconia Alloy: I. Deformation and Fracture Observations," *J. Am. Ceram. Soc.* **72** [1] 90–98 (1989).

[3]L. R. F. Rose and M. V. Swain, "Transformation Zone Shape in Ceria-Partially-Stabilized Zirconia," *Acta Metall.*, **36** [4] 955–62 (1988).

[4]C.-S. Yu and D. K. Shetty, "Transformation Zone Shape, Size, and Crack-Growth-Resistance (*R*-curve) Behavior of Ceria-Partially Stabilized Zirconia Polycrystals," *J. Am. Ceram. Soc.*, **72** [6] 921–28 (1989).

[5]P. E. Reyes-Morel and I-W. Chen, "Transformation Plasticity of CeO_2-Stabilized Tetragonal Zirconia Polycrystals: I. Stress Assistance and Autocatalysis," *J. Am. Ceram. Soc.*, **72** [5] 343–53 (1988).

[6]P. E. Reyes-Morel, J.-S. Cherng, and I-W. Chen, "Transformation Plasticity of CeO_2-Stabilized Tetragonal Zirconia Polycrystals: II. Pseudoelasticity and Shape Memory Effect," *J. Am. Ceram. Soc.*, **71** [8] 648–57 (1988).

[7]K. E. Tsukuma and M. Shimada, "Strength, Fracture Toughness, and Vickers Hardness of CeO_2-Stabilized Tetragonal Zirconia Polycrystals (Ce-TZP)," *J. Mater. Sci.*, **204** [4] 1178–84 (1985).

[8]T. Sato, T. Endo, and M. Shimada, "Postsintering Hot Isostatic Pressing of Ceria-Doped Tetragonal Zirconia/Alumina Composites in an Argon–Oxygen Gas Atmosphere," *J. Am. Ceram. Soc.*, **72** [5] 761–64 (1989).

[9]D. B. Marshall, M. C. Shaw, R. H. Dauskardt, R. O. Ritchie, M. Readey, and A. H. Heuer, "Crack-Tip Transformation Zones in Toughened Zirconia," *J. Am. Ceram. Soc.*, **73** [9] 2659–66 (1990).

[10]R. M. McMeeking and A. G. Evans, "Mechanics of Transformation Toughening in Brittle Materials," *J. Am. Ceram. Soc.*, **65** [5] 242–46 (1982).

[11]D. B. Marshall, A. G. Evans, and M. Drory, "Transformation Toughening in Ceramics", p. 289 in Fracture Mechanics of Ceramics, Vol. 6. Edited by R. C. Bradt, A. G. Evans, D. P. H. Hasselman, and F. F. Lange. Plenum Press, New York, 1983.

[12]D. B. Marshall and M. V. Swain, "Crack Resistance Curves in Magnesia-Partially-Stabilized Zirconia," *J. Am. Ceram. Soc.*, **71** [6] 399–407 (1988).

[13]A. H. Heuer, M. Rühle, and D. B. Marshall, "On the Thermoelastic Martensitic Transformation in Tetragonal ZrO_2," *J. Am. Ceram. Soc.*, **73** [4] 1084–93 (1990).

[14]J.-F. Tsai, C.-S. Yu, and D. K. Shetty, "Autocatalytic Transformation and the Zone Shape in Ceria-Partially-Stabilized Zirconia (Ce-TZP)"; unpublished work. □

6.0 ENHANCED FRACTURE TOUGHNESS IN LAYERED Ce-ZrO_2/Al_2O_3 MICROSTRUCTURES

To be submitted to J. Am. Ceram. Soc.

LAYERED COMPOSITES OF Ce-ZrO_2 and Al_2O_3

D.B. Marshall and J.J. Ratto
Rockwell International Science Center
1049 Camino Dos Rios
Thousand Oaks, CA 91360

F.F. Lange
Materials Department
University of California
Santa Barbara, CA 93106

ABSTRACT

Laminar composites, containing layers of Ce-TZP and either Al_2O_3 or a mixture of Al_2O_3 and Ce-ZrO_2, have been fabricated using a colloidal method that allowed layer thicknesses as small as 10 μm. Strong interactions between these layers and the transformation zones surrounding cracks and indentations have been observed. Transformation zones surrounding cracks are increased in width, resulting in enhanced fracture toughness.

1. INTRODUCTION

High fracture toughnesses, in the range 10-20 MPa•$m^{1/2}$, have been achieved recently in ceria-partially-stablized zirconia (Ce-TZP) that undergoes martensitic transformation from tetragonal to monoclinic phase.[1-7] However, the shapes of the transformation zones surrounding cracks in these materials are not optimal for producing large transformation toughening.[8] Whereas in other zirconia ceramics of comparable toughness (magnesia-partially-stabilized zirconia, Mg-PSZ), the transformation zone extends approximately equal distances ahead and to the side of a crack,[9] the zone in Ce-TZP is very elongated, extending ahead of the crack a distance of 10 to 20 times the zone width.[1-4] The extra transformed material ahead of the crack degrades the toughness; calculation of the crack tip shielding from zones with such shapes indicates that the increase in fracture toughness due to transformation shielding is about a factor of 2 smaller for an elongated frontal zone typical of Ce-TZP than for a semicircular frontal zone shape characteristic of Mg-PSZ.[8] Therefore, substantial benefit should result if the microstructure of Ce-TZP could be modified to change the shape of the transformation zone.

The elongated frontal zone in Ce-TZP is thought to result from autocatalytic transformation, i.e., the sequential triggering of transformation in a grain by transformation strains in adjacent grains. Autocatalytic transformation also occurs in Mg-PSZ, as evidenced by the formation of well-defined shear bands within grains.[10] The microstructure of Mg-PSZ may be thought of as dual scale; the individual precipitates that transform from tetragonal to monoclinic phase are lenticular in shape (~ 300 nm in diameter) and are contained within grains that are larger by about 2 orders of magnitude (~ 50 μm diameter).[11] Although each transformation band contains many autocatalyti-

cally transformed precipitates, the grain boundaries are effective as barriers, which arrest the propagating band. In Ce-TZP, there is no such large scale barrier to arrest a developing transformation band; in this case, the transforming units are the individual grains and there is no larger scale microstructural unit.

In this paper, we describe an approach for introducing a large-scale microstructural unit into Ce-TZP, in the form of layers of either Al_2O_3 or a mixture of Al_2O_3 and Ce-TZP. Based on the above discussion, the optimum separation of the layers would be expected to be a factor of ~ 10-100 times the grain size (which is ~ 2 μm), with individual layer thicknesses being at the lower end of the range. Layered structures satisfying this requirement have been fabricated using a colloidal method to consolidate powders. This approach has allowed formation of layers as thin as ~ 10 μm, considerably smaller than the layer thicknesses produced by conventional tape casting methods for multilayer structures. Controlled crack growth experiments and indentation experiments are used to investigate the influence of these barrier layers on crack tip transformation zones.

2. COMPOSITE FABRICATION

Composites of Ce-ZrO_2 with layers of either Al_2O_3 or a mixture of 50% Al_2O_3-50% Ce-ZrO_2 were fabricated using a colloidal technique. The technique involved sequential centrifuging of solutions containing suspended particles to form the layered green body, followed by drying and sintering at 1600°C for 3 h. Use was made of a technique described recently by Velamakanni et. al.,[12] in which an aqueous electrolyte (NH_4NO_3) was used to cause hydration repulsion forces between individual suspended particles, in order to counteract the van der Waals attraction and thereby prevent

flocculation. Under these conditions, the particles aggregate weakly with a lubricating film of liquid between them, thus allowing rearrangement and packing to high green density without mass separation.

The relative green densities of the Al_2O_3 and Ce-ZrO_2 powders‡ consolidated separately in this manner were 60% and 50%, respectively. The subsequent larger shrinkage of the Ce-ZrO_2 during sintering caused cracking in most layered composites that contained pure Al_2O_3 layers (the exceptions being some very thin layers, < 20 μm thickness). This mismatch was avoided by using the mixed composition 50% Al_2O_3-50% $CeZrO_2$ instead of pure Al_2O_3.

The Ce-ZrO_2 powder used in this preliminary study yields a material of intermediate fracture toughness (K_c ~ 8 MPa•$m^{1/2}$). The widths of transformation zones surrounding cracks are approximately 15 μm, as determined by Nomarski interference observations of surface distortion due to the transformation strains. This is substantially smaller than the zone sizes observed in more transformable Ce-ZrO_2 materials (several hundred microns).[2-4]

3. MICROSTRUCTURAL OBSERVATIONS

Optical micrographs of typical layers of 50% Al_2O_3-50% $CeZrO_2$ within a matrix of Ce-ZrO_2 are shown in Fig. 1. Reasonably uniform layers with thicknesses in the range 10 to 100 μm were readily formed. A multilayered structure of alternating Ce-ZrO_2 and 50% Al_2O_3-50% Ce-ZrO_2 layers of thickness 20 μm is shown in Fig. 1(b).

---

‡ Al_2O_3 powder from Sumitomo.
Ce-TZP powder from Tosoh, Tokyo, grade TZ-12Ce.

4. MECHANICAL PROPERTIES

4.1 The Role of Isolated Layers

The influence of individual layers of Al_2O_3 or 50% Al_2O_3-50% $CeZrO_2$ on crack growth and transformation zones in Ce-ZrO_2 was investigated by fabricating composites containing widely spaced layers. Measurements were obtained from controlled crack growth in notched beams, fracture of smooth bars, and indentation experiments using a Vickers indenter.

Observations from a notched beam loaded in bending are shown in Fig. 2. A crack was grown from the notch by loading the beam in bending using a fixture on the stage of an optical microscope, which allowed high magnification observations of the sides of the beam during crack growth, with continuous load measurements. The results shown in Fig. 2 were obtained from a specimen containing three layers of 50% Al_2O_3-50% $CeZrO_2$ widely spaced ahead of the notch, as shown in Fig. 2(a). After initiating stably in the immediate vicinity of the notch, the crack grew unstably and arrested approximately 20 μm before the first layer of Al_2O_3/ZrO_2, which had thickness ~ 35 μm. The width of the transformation zone over the wake of the crack, as determined by Nomarski interference, was approximately 15 μm. However, near the tip of the arrested crack, the transformation zone extended adjacent to the Al_2O_3/ZrO_2 layer for distances of more than 150 μm each side of the crack, as shown in Figs. 2(b) and (c). Some transformation also occurred on the opposite side of the Al_2O_3/ZrO_2 layer, also for a distance of 150 μm both sides of the crack plane.

After further loading, the crack grew unstably through the Al_2O_3/ZrO_2 layer, into the $CeZrO_2$ on the opposite side, and arrested again ~ 40 μm before the second layer,

which had a thickness of 70 μm. The shape of the transformation zone along the layer near the crack tip was similar to that at the first arrest position (Figs. 2(b) and (c). Optical interference micrographs of regions around the first and second layers, with the crack tip at this position are shown in Figs. 2(c) and (e). These results indicate that the Al_2O_3/ZrO_2 barrier layers have a much larger effect than simply arresting the growth of a transformation zone ahead of a crack; they also promote expansion of the zone to the side of the crack, which is the location that gives rise to crack tip shielding and hence toughening.

Smooth beams of the same composite as in Fig. 2 were broken in bending in the two orientations shown in Fig. 3(a) and (b). In the orientation of Fig. 3(a), which is the same as that of the notched beam, failure occurred unstably at a critical load. The polished side surfaces of the beams exhibited similar evidence for widening of the transformation zone near the Al_2O_3/ZrO_2 layers as in Figs. 2(b) to (e). Therefore, this beneficial interaction appears to occur for fast moving as well as for stable cracks. In the orientation of Fig. 3(b), fracture also initiated unstably from the tensile surface at a critical load. However, the crack arrested before it reached the opposite side, leaving the beam intact (Fig. 3(c)). The effectiveness of the Al_2O_3/ZrO_2 layers in arresting this crack is especially noteworthy since there were only two layers in the beam, accounting for 2% of its volume. On the surface that had been loaded in tension, there were several narrow bands of transformed material in addition to the crack that caused the sudden load drop, similar to observations in the literature (Fig. 3(d)). However, some of the transformation bands were arrested at the Al_2O_3/ZrO_2 layers. There is also evidence that the crack itself arrested at the Al_2O_3/ZrO_2 layer before joining with a second crack to cause failure.

Vickers indentations in the Ce-TZP were surrounded by large zones of transformed material, which caused uplift of the surface adjacent to the indentations. Micrographs, obtained using both Nomarski interference and conventional interference, of several such zones in the vicinities of Al_2O_3/ZrO_2 layers are shown in Fig. 4. At indentation loads up to 300N, there was no cracking caused by the indentations. The presence of a nearby Al_2O_3/ZrO_2 layer within the transformation zone caused spreading the zone in the region adjacent to the layer, in a pattern that is similar to the crack tip zone spreading of Fig. 2. There was also transformed material on the side opposite the indentation. The surface uplift, measured from the optical interference micrograph of Fig. 4, is plotted in Fig. 5 along several lines near the indentation, as depicted in the inset of Fig. 5. The presence of the Al_2O_3/ZrO_2 layer caused substantially larger uplift everywhere on the side of the indentation that is closer to the layer. The surface of the Al_2O_3/ZrO_2 layer is depressed relative to the adjacent transformed Ce-ZrO_2 material. However, this Al_2O_3/ZrO_2 layer is uplifted more than the Ce-ZrO_2 surface at corresponding positions on the opposite side of the indentation. This observation provides evidence that the Al_2O_3/ZrO_2 layer caused spreading of the transformation zone adjacent to the layer in the depth direction as well as along the surface, and/or a larger concentration of transformed material in the region adjacent to the layer.

4.2 The Response of Multilayered Structures

The influence of multilayered structures on transformation zone shapes was investigated using a specimen shown schematically in Fig. 6(a), containing 19 layers of alternating Ce-TZP and Al_2O_3/ZrO_2, each of 35 μm thickness, in the center of a beam of Ce-TZP. Optical interference micrographs (Fig. 6(b)) show that the width of the

transformed zone adjacent to the crack is about a factor of 10 larger (~ 150 μm) within the multilayered region than in the Ce-TZP (~ 15 μm). Moreover, even though the uplift is constrained by the presence of the higher stiffness Al_2O_3/ZrO_2 layer, and the average volume fraction of Ce-TZP is lower in the layered region, the magnitude of the surface uplift adjacent to the crack, as measured from optical micrographs such as Fig. 6(b), is larger by a factor of about 2 within the layered region than in the Ce-TZP.

5. DISCUSSION

The results in Section 4 show that the presence of Al_2O_3 or Al_2O_3/ZrO_2 layers in Ce-TZP has a large effect in spreading transformation zones along the regions adjacent to the layers. The spreading is driven by the constraint due to the nontransformability of the layers and their higher elastic stiffness. However, the mechanics of the spreading has not been analyzed in detail.

If the layers are oriented normal to the plane of a crack, the spreading of the transformation zone must result in increased crack shielding, and thus higher fracture toughness. For a multilayered composite such as that shown in Fig. 6, the toughening can be crudely estimated from the measured zone widths and surface uplift. Since the toughness increase is proportional to $f\sqrt{w}$, where f is the concentration of transformed material and w is the zone width, the observed increase in w by a factor of 10, with an allowance for f to decrease by a factor of 2 (assuming conservatively that no transformation occurs in the Al_2O_3/ZrO_2 layer), would give rise to an increase in fracture toughness of 50%. This estimate is also consistent with the observed surface uplift; with the result of a previous study,[9] which found experimentally that the toughness increase is proportional to the square root of the surface uplift adjacent to the

crack, the observed increase in uplift by a factor of 2 in the multilayered region would imply a toughness increase of ~ 40%.

The toughening due to spreading of the transformation zone acts in addition to the predicted toughening due to elimination of the elongated frontal zone. In high toughness Ce-TZP ($K_c \approx$ 20 MPa•$m^{1/2}$), the zone spreading through the use of Al_2O_3/ZrO_2 could increase the toughness in a multilayered composite to ~ 28 MPa•$m^{1/2}$ (allowing 4 MPa for the base toughness of the Ce-ZrO_2 without transformation toughening), whereas elimination of the frontal zone could increase this further to 48 MPa•$m^{1/2}$. Therefore, the potential exists for such composites to exhibit fracture toughnesses substantially higher than observed in any other ceramic material.

ACKNOWLEDGEMENT

Funding for this work was provided by the U.S. Air Force Office of Scientific Research under Contract No. F49620-89-C-0031.

REFERENCES

1. M.V. Swain, R.H.J. Hannink and J. Drennan, "Some Interfacial Related Properties of Transformation Toughened Ceramics," p. 819 in Ceramic Microstructures '86, Role of Interfaces, ed., J.A. Pask and A.G. Evans.

2. R.H.J. Hannink and M.V. Swain, "Metastability of Martensitic Transformation in a 12 mol.% Ceria-Zirconia Alloy: Deformation and Fracture Observations," J. Am. Ceram. Soc. 72[1], 90-98 (1989).

3. L.R.F. Rose and M.V. Swain, "Transformation Zone Shape in Ceria-Partially-Stabilized Zirconia," Acta. Metall. 36[4], 955-962 (1988).

4. C-S Yu and D.K. Shetty, "Transformation Zone, Shape, Size and Crack-Growth-Resistance (R-curve) Behavior of Ceria-Partially Stabilized Zirconia Polycrystals," J. Am. Ceram. Soc. 72[6], 921-28 (1989).

5. P.E. Reyes-Morel and I-W Chen, "Transformation Plasticity of CeO_2-Stabilized Tetragonal Zirconia Polycrystals: I, Stress Assistance and Autocatalysis," J. Am. Ceram. Soc. 72[5], 343-53 (1988).

6. P.E. Reyes-Morel, J-S Cherng and I-W Chen, "Transformation Plasticity of CeO_2-Stabilized Tetragonal Zirconia Polycrystals: II, Pseudoelasticity and Shape Memory Effects," J. Am. Ceram. Soc. 71[8], 648-57 (1988).

7. K.E. Tsukuma and M. Shimada, "Strength, Fracture Toughness, and Vickers Hardness of CeO_2-Stabilized Tetragonal Zirconia Polycrystals (Ce-TZP)," J. Mat. Sci. 204[4], 1178-84 (1985).

8. D.B. Marshall, "Crack Shielding in Ceria-Partially-Stabilized Zirconia," J. Am. Ceram. Soc. 73[10], 3119-21 (1990).

9. D.B. Marshall, M.C. Shaw, R.H. Dauskardt, R.O. Ritchie, M. Readey and A.H. Heuer, "Crack Tip Transformation Zones in Toughened Zirconia," J. Am. Ceram. Soc., 73[9], 2659-66 (1990).

10. A.H. Heuer, M. Rühle and D.B. Marshall, "On the Thermoelastic Transformation in Tetragonal ZrO_2," J. Am. Ceram. Soc. 73[4], 1084-93 (1990).

11. R.H.J. Hannink and M.V. Swain, "Magnesia-Partially Stabilized Zirconia: The Influence of Heat Treatment on Thermomechanical Properties," J. Aust. Ceram. Soc. 18[2], 53-62 (1982).

12. B.V. Velamakanni, J.C. Chang, F.F. Lange and D.S. Pearson, "A New Method for Efficient Colloidal Particle Packing Via Modulation of Repulsive Lubricating Hydration Forces," Langmuir, in press.

FIGURE CAPTIONS

Fig. 1 Optical micrographs showing layered ZrO_2 microstructures.

(a) Isolated layers of Al_2O_3/Ce-ZrO_2 (darker regions) of various thickness in a matrix of Ce-TZP.

(b) Multilayered structure with alternating Ce-TZP and Al_2O_3/Ce-TZP layers of thickness 35 μm.

Fig. 2 (a) Schematic of notched beam of Ce-TZP containing several layers of Al_2O_3/Ce-ZrO_2.

(b) Nomarski interference micrograph showing arrested crack tip near Al_2O_3/ZrO_2 layer (as indicated in (a)) with widened transformation zone adjacent to layer.

(c) Optical interference micrograph of area in (b). Reference mirror is parallel to surface remote from crack, so that fringes represent contours of constant surface uplift (due to transformation strains).

(d) and (e) Micrographs taken as in (b) and (c) from the region in the crack wake near the first Al_2O_3/ZrO_2 layer, as indicated in (a).

Fig. 3 (a) and (b) Bending test geometry showing orientations of Al_2O_3/ZrO_2 layers relative to bending direction.

(c) Side view of crack in specimen oriented as in (b), showing crack arrest before complete failure.

(d) Tensile surface of specimen from (c) showing crack arrest at Al_2O_3/ZrO_2 layer and arrest of transformation bands at the Al_2O_3/ZrO_2 layer (note the transformation band can also be seen on the side surface in (c)).

Fig. 4 Vickers indentations (200 N load) near layers of Al_2O_3 and Al_2O_3/ZrO_2 showing interaction of layers with transformation zone.

(a) Nomarski interference, Al_2O_3/ZrO_2 layer 30 μm thickness.

(b)-(d) Optical interference micrographs with reference mirror parallel to specimen surface remote from indentations, (fringes represent contours of surface uplift): (b) Al_2O_3/ZrO_2 layer 30 μm thickness, (c) Al_2O_3 layer 30 μm thickness, and (d) Al_2O_3 layer 10 μm thickness.

Fig. 5 Surface uplift measured from Fig. 4(b) along four paths as indicated.

Fig. 6 (a) Multilayered region embedded within a matrix of Ce-TZP.

(b) Optical interference micrograph of specimen depicted in (a) after growing crack from notch, showing larger transformation zone width in multilayered region than in Ce-TZP.

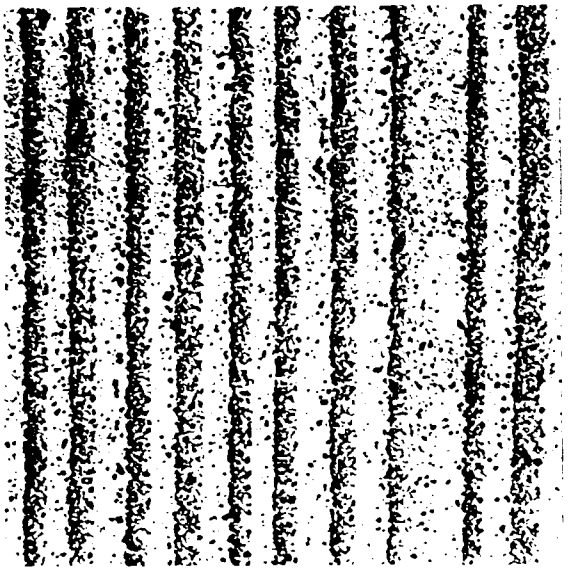

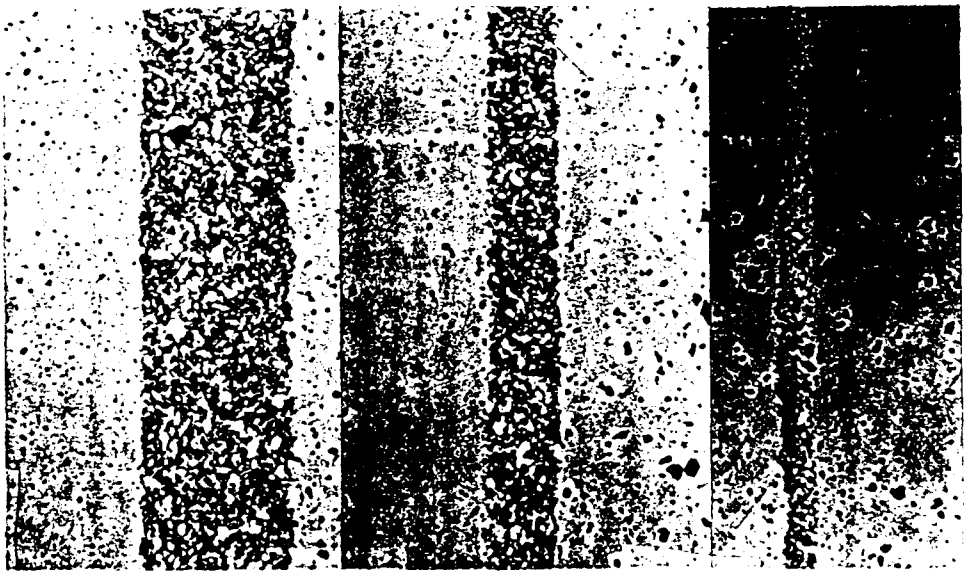

FIG. 2 (a)

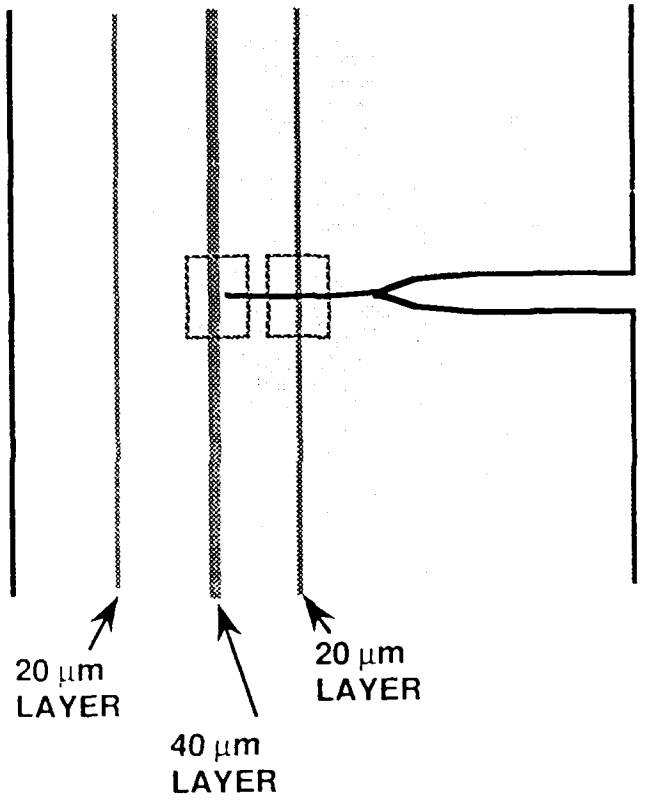

FIG. 2 (a)

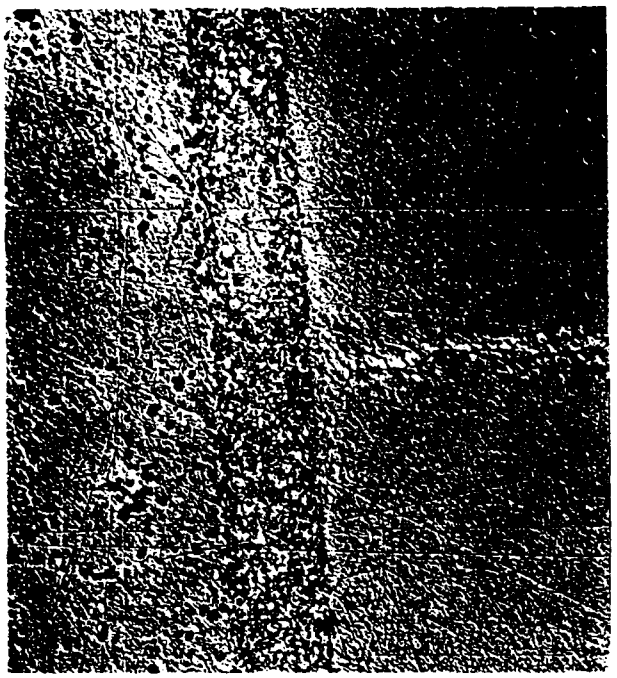

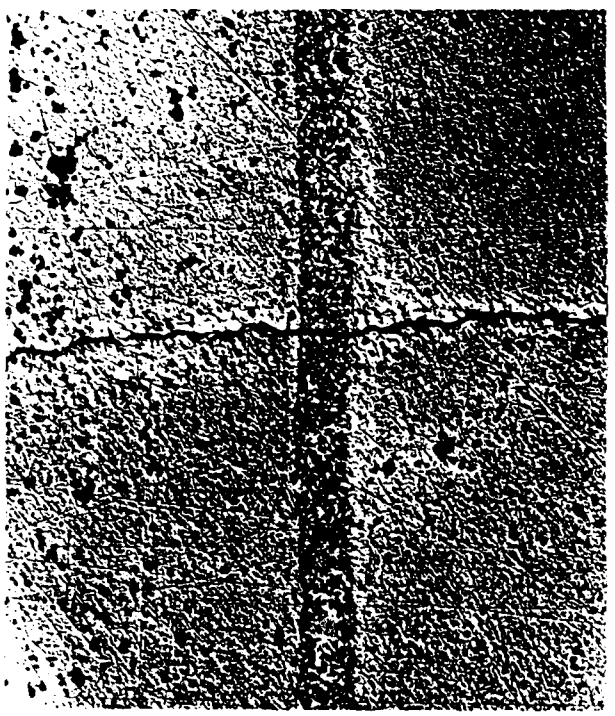

2 (b) - (e)

FIG. 3 (a,b)

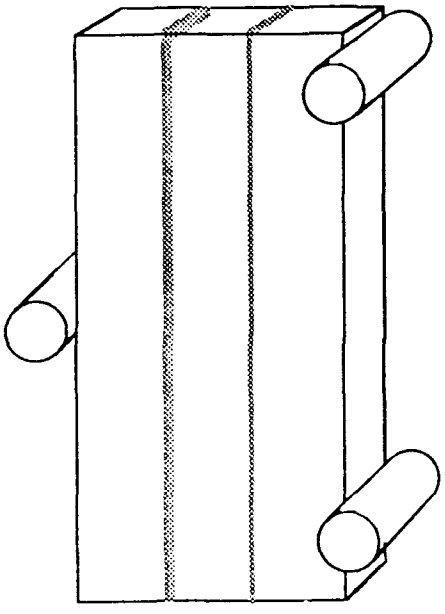

(a)

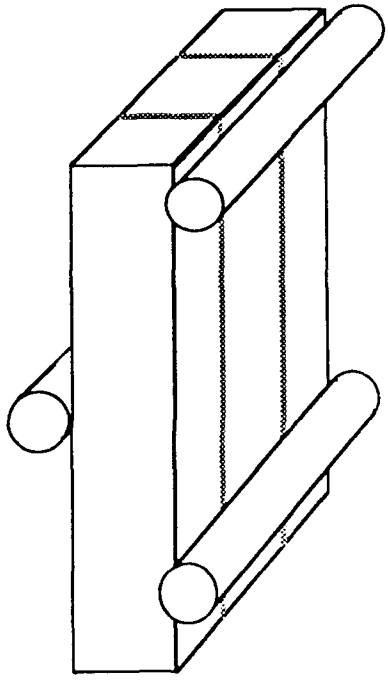

(b)

FIG. 3 (a,b)

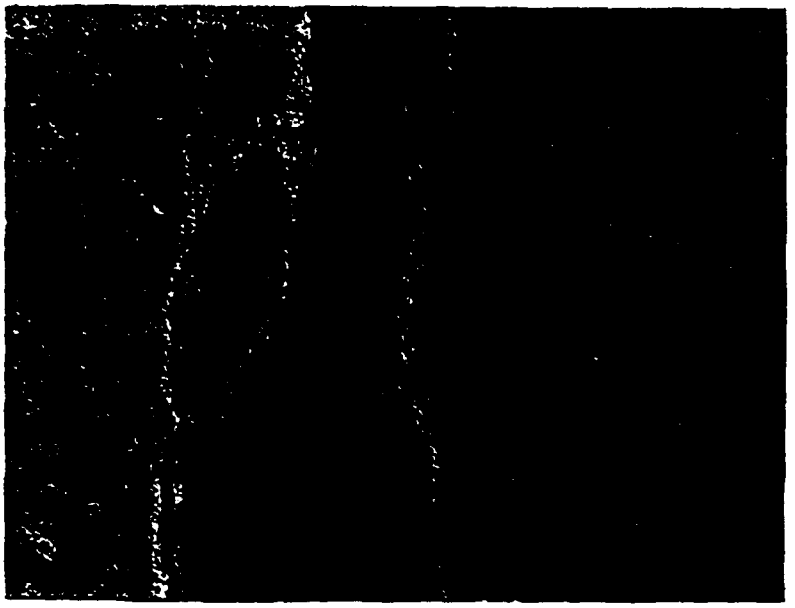

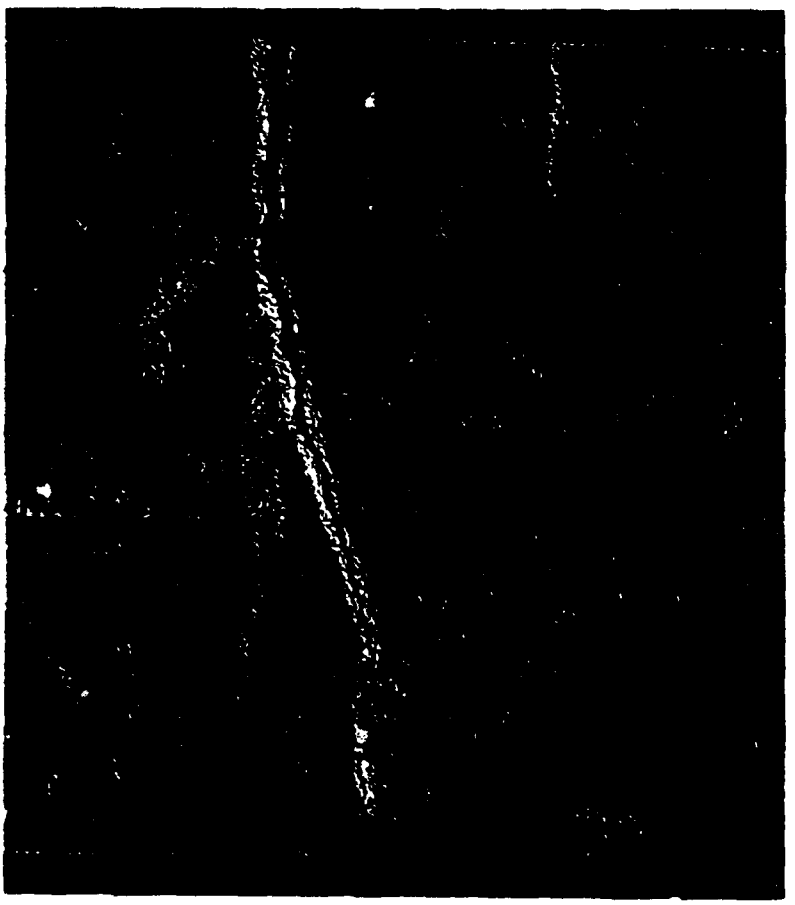

3(c)(d)

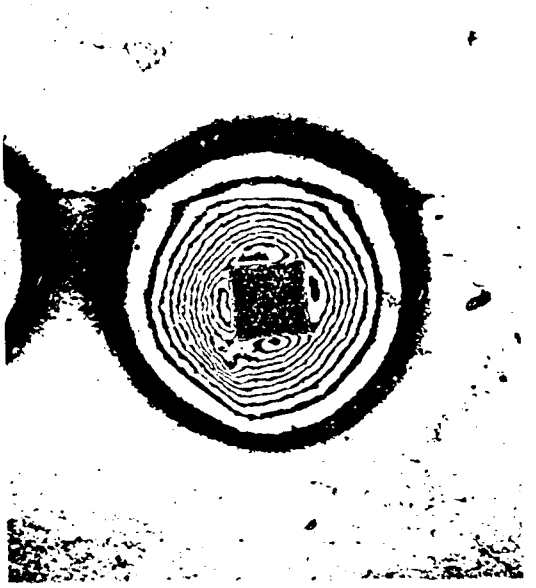

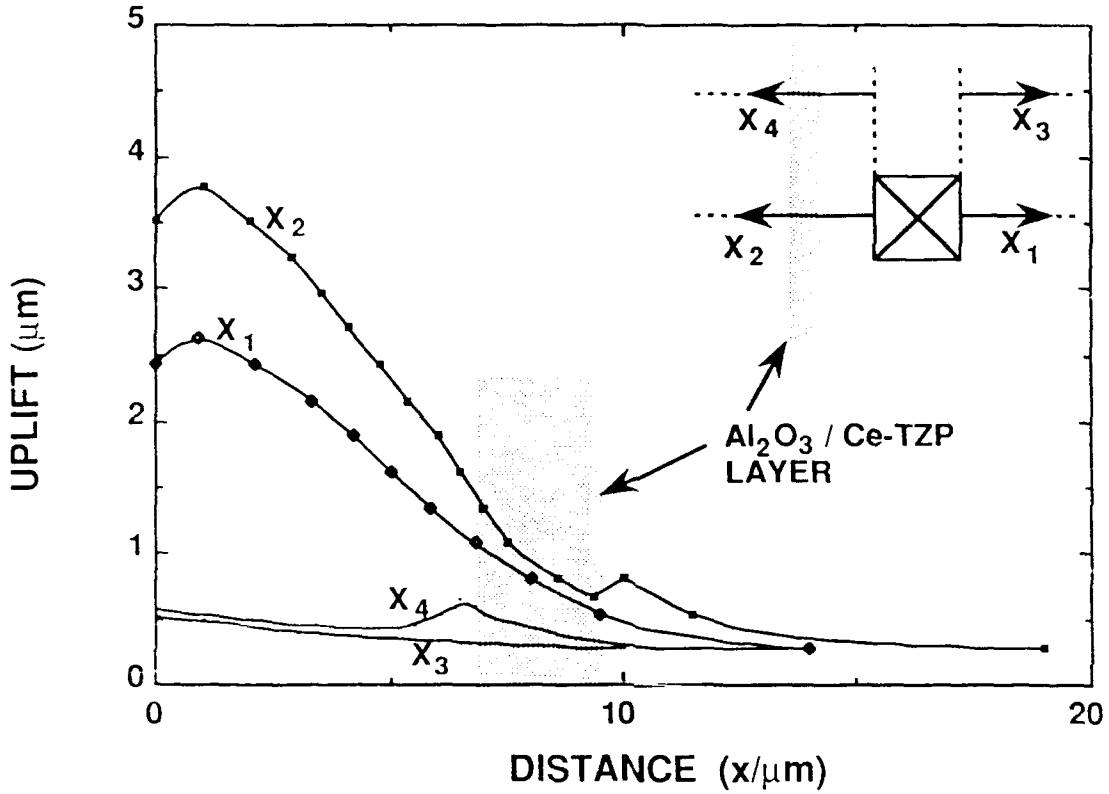
UPLIFT (μm)
DISTANCE (x/μm)
0
1
2
3
4
5
0
10
20
X1
X2
X3
X4
Al2O3 / Ce-TZP
LAYER

FIG. 6 (a)